

MHD Turbulence: Scaling Laws and Astrophysical Implications

Jungyeon Cho¹, A. Lazarian¹, and Ethan T. Vishniac²

¹ Univ. of Wisconsin, Madison WI53706, USA

² Johns Hopkins Univ., Baltimore MD21218, USA

Abstract. Turbulence is the most common state of astrophysical flows. In typical astrophysical fluids, turbulence is accompanied by strong magnetic fields, which has a large impact on the dynamics of the turbulent cascade. Recently, there has been a significant breakthrough on the theory of magnetohydrodynamic (MHD) turbulence. For the first time we have a scaling model that is supported by both observations and numerical simulations. We review recent progress in studies of both incompressible and compressible turbulence. We compare Iroshnikov-Kraichnan and Goldreich-Sridhar models, and discuss scalings of Alfvén, slow, and fast waves. We also discuss the completely new regime of MHD turbulence that happens below the scale at which hydrodynamic turbulent motions are damped by viscosity. In the case of the partially ionized diffuse interstellar gas the viscosity is due to neutrals and truncates the turbulent cascade at \sim parsec scales. We show that below this scale magnetic fluctuations with a shallow spectrum persist and discuss the possibility of a resumption of the MHD cascade after ions and neutrals decouple. We discuss the implications of this new insight into MHD turbulence for cosmic ray transport, grain dynamics, etc., and how to test theoretical predictions against observations.

1 Introduction

Most astrophysical systems, e.g. accretion disks, stellar winds, the interstellar medium (ISM) and intercluster medium are turbulent with an embedded magnetic field that influences almost all of their properties. This turbulence which spans from km to many kpc (see discussion in [2,150,86]) holds the key to many astrophysical processes (e.g., transport of mass and angular momentum, star formation, fragmentation of molecular clouds, heat and cosmic ray transport, magnetic reconnection). Statistics of turbulence is also essential for the cosmic microwave background (CMB) radiation foreground studies [88].

All turbulent systems have one thing in common: they have a large “Reynolds number” ($Re \equiv LV/\nu$; L = the characteristic scale or driving scale of the system, V =the velocity difference over this scale, and ν =viscosity), the ratio of the viscous drag time on the largest scales (L^2/ν) to the eddy turnover time of a parcel of gas (L/V). A similar parameter, the “magnetic Reynolds number”, Rm ($\equiv LV/\eta$; η =magnetic diffusion), is the ratio of the magnetic field decay time (L^2/η) to the eddy turnover time (L/V). The properties of the flows on all scales depend on Re and Rm . Flows with $Re < 100$ are laminar; chaotic structures develop gradually as Re increases, and those with $Re \sim 10^3$ are appreciably less

chaotic than those with $Re \sim 10^7$. Observed features such as star forming clouds and accretion disks are very chaotic with $Re > 10^8$ and $Rm > 10^{16}$.

Let us start by considering incompressible hydrodynamic turbulence, which can be described by the Kolmogorov theory [68]. Suppose that we excite fluid motions at a scale L . We call this scale the *energy injection scale* or the *largest energy containing eddy scale*. For instance, an obstacle in a flow excites motions on scales of the order of its size. Then the energy injected at the scale L cascades to progressively smaller and smaller scales at the eddy turnover rate, i.e. $\tau_l^{-1} \approx v_l/l$, with negligible energy losses along the cascade ¹. Ultimately, the energy reaches the molecular dissipation scale l_d , i.e. the scale where the local $Re \sim 1$, and is dissipated there. The scales between L and l_d are called the *inertial range* and it typically covers many decades. The motions over the inertial range are *self-similar* and this provides tremendous advantages for theoretical description.

The beauty of the Kolmogorov theory is that it does provide a simple scaling for hydrodynamic motions. If the velocity at a scale l from the inertial range is v_l , the Kolmogorov theory states that the kinetic energy ($\rho v_l^2 \sim v_l^2$ as the density is constant) is transferred to next scale within one eddy turnover time (l/v_l). Thus within the Kolmogorov theory the energy transfer rate ($v_l^2/(l/v_l)$) is scale-independent,

$$\frac{v_l^2}{t_{cas}} \sim \frac{v_l^2}{(l/v_l)} = \text{constant}, \quad (1)$$

and we get the famous Kolmogorov scaling

$$v_l \propto l^{1/3}. \quad (2)$$

The one-dimensional² energy spectrum $E(k)$ is the amount of energy between the wavenumber k and $k+dk$ divided by dk . When $E(k)$ is a power law, $kE(k)$ is the energy *near* the wavenumber $k \sim 1/l$. Since $v_l^2 \approx kE(k)$, Kolmogorov scaling implies

$$E(k) \propto k^{-5/3}. \quad (3)$$

Kolmogorov scalings were the first major advance in the theory of incompressible turbulence. They have led to numerous applications in different branches of science (see [112]). However, astrophysical fluids are magnetized and the a dynamically important magnetic field should interfere with eddy motions.

Paradoxically, astrophysical measurements are consistent with Kolmogorov spectra (see LPE02 [86]). For instance, interstellar scintillation observations indicate an electron density spectrum is very close to $-5/3$ for $10^8 \text{cm} - 10^{15} \text{cm}$ (see [2]). At larger scales LPE02 summarizes the evidence of $-5/3$ velocity power spectrum over pc-scales in HI. Solar-wind observations provide *in-situ* measurements of the power spectrum of magnetic fluctuations and Leamon et al. [93] also obtained a slope of $\approx -5/3$. Is this a coincidence? What properties is the magnetized compressible ISM expected to have? We will deal with these questions, and some related issues, below.

¹ This is easy to see as the motions at the scales of large eddies have $Re \gg 1$.

² Dealing with observational data, e.g. in LPE02 [86], we deal with three dimensional energy spectrum $P(k)$, which, for isotropic turbulence, is given by $E(k) = 4\pi k^2 P(k)$.

Our approach here is complementary to that in Vazquez-Semadeni (this volume) and Mac Low (this volume). These reviews discuss attempts to simulate the turbulent ISM in all its complexity by including many physical processes (e.g. heating, cooling, self-gravity) simultaneously. This provides a possibility of comparing observations and simulations (see review by Ostriker, this volume). The disadvantage is that such simulations cannot distinguish between the consequences of different processes. Note, that in studies of turbulence the adaptive mesh does not help as the fine structures emerge through the entire computational volume.

Here we discuss a focused approach which aims at obtaining a clear understanding on the fundamental level, and considering physically relevant complications later. The creative synthesis of both approaches is the way, we think, that studies of astrophysical turbulence should proceed³. Certainly an understanding of MHD turbulence in the most ideal terms is a necessary precursor to understanding the complications posed by more realistic physics and numerical effects. For review of general properties of MHD, see a recent book by Biskamp [5].

In what follows, we first consider observational data that motivate our study (§2), then discuss theoretical approaches to incompressible MHD turbulence (§3). In §4 we discuss testing and extending of the Goldreich-Sridhar theory of turbulence, then in §5 we deal with viscous damping of incompressible turbulence and describe a new regime of MHD turbulence that is present below the viscous cut-off scale. We move to the effects of compressibility in §6 and discuss implications of our new understanding of MHD turbulence for the problems of dust motion, cosmic ray dynamics, support of molecular clouds, heating of ISM etc in §7. We propose observational testing of our results in §8 and present the summary in §9.

2 Observational Data

Kolmogorov turbulence is the simplest possible model of turbulence. Since it is incompressible and not magnetized, it is completely specified by its velocity spectrum. If a passive scalar field, like “dye particles” or temperature inhomogeneities, is subjected to Kolmogorov turbulence, the resulting spectrum of the passive scalar density is also Kolmogorov (see [95,171]). In compressible and magnetized turbulence this is no longer true, and a complete characterization of the turbulence requires not only a study of the velocity statistics but also the statistics of density and magnetic fluctuations.

³ Potentially our approach leads to an understanding of the relationship between motions at a given time at small scales (subgrid scales) and the state of the flow at a previous time at some larger, resolved, scale. This could lead to a parametrization of the subgrid scales and to large eddy simulations of MHD.

Direct studies of turbulence⁴ have been done mostly for interstellar medium and for the Solar wind. While for the Solar wind *in-situ* measurements are possible, studies of interstellar turbulence require inverse techniques to interpret the observational data.

Attempts to study interstellar turbulence with statistical tools date as far back as the 1950s [59,64,117,172] and various directions of research achieved various degree of success (see reviews by [65,31,2,78,79,86]).

2.1 Solar wind

Solar wind (see review [48]) studies allow pointwise statistics to be measured directly using spacecrafts. These studies are the closest counterpart of laboratory measurements.

The solar wind flows nearly radially away from the Sun, at up to about 700 km/s. This is much faster than both spacecraft motions and the Alfvén speed. Therefore, the turbulence is “frozen” and the fluctuations at frequency f are directly related to fluctuations at the scale k in the direction of the wind, as $k = 2\pi f/v$, where v is the solar wind velocity [57].

Usually two types of solar wind are distinguished, one being the fast wind which originates in coronal holes, and the slower bursty wind. Both of them show, however, $f^{-5/3}$ scaling on small scales. The turbulence is strongly anisotropic (see [66]) with the ratio of power in motions perpendicular to the magnetic field to those parallel to the magnetic field being around 30. The intermittency of the solar wind turbulence is very similar to the intermittency observed in hydrodynamic flows [58].

2.2 Electron density statistics

Studies of turbulence statistics of ionized media (see [157]) have provided information on the statistics of plasma density at scales 10^8 - 10^{15} cm. This was based on a clear understanding of processes of scintillations and scattering achieved by theorists⁵ (see [121,49]). A peculiar feature of the measured spectrum (see [2]) is the absence of the slope change at the scale at which the viscosity by neutrals becomes important.

Scintillation measurements are the most reliable data in the “big power law” plot in Armstrong et al. [2]. However there are intrinsic limitations to the scintillations technique due to the limited number of sampling directions, its relevance only to ionized gas at extremely small scales, and the impossibility of getting velocity (the most important!) statistics directly. Therefore with the data one faces the problem of distinguishing actual turbulence from static density structures.

⁴ Indirect studies include the line-velocity relationships [75] where the integrated velocity profiles are interpreted as the consequence of turbulence. Such studies do not provide the statistics of turbulence and their interpretation is very model dependent.

⁵ In fact, the theory of scintillations was developed first for the atmospheric applications.

Moreover, the scintillation data does not provide the index of turbulence directly, but only shows that the data are consistent with Kolmogorov turbulence. Whether the (3D) index can be -4 instead of -11/3 is still a subject of intense debate [56,121]. In physical terms the former corresponds to the superposition of random shocks rather than eddies.

Additional information on the electron density is contained in the Faraday rotation measures of extragalactic radio sources (see [154,155]). However, there is so far no reliable way to disentangle contributions of the magnetic field and the density to the signal. We feel that those measurements may give us the magnetic field statistics when we know the statistics of electron density better.

2.3 Velocity and density statistics from spectral lines

Spectral line data cubes are unique sources of information on interstellar turbulence. Doppler shifts due to supersonic motions contain information on the turbulent velocity field which is otherwise difficult to obtain. Moreover, the statistical samples are extremely rich and not limited to discrete directions. In addition, line emission allows us to study turbulence at large scales, comparable to the scales of star formation and energy injection.

However, the problem of separating velocity and density fluctuations within HI data cubes is far from trivial [77,79,84,86]. The analytical description of the emissivity statistics of channel maps (velocity slices) in Lazarian & Pogosyan [84] (see also [79,86] for reviews) shows that the relative contribution of the density and velocity fluctuations depends on the thickness of the velocity slice. In particular, the power-law asymptote of the emissivity fluctuations changes when the dispersion of the velocity at the scale under study becomes of the order of the velocity slice thickness (the integrated width of the channel map). These results are the foundation of the Velocity-Channel Analysis (VCA) technique which provides velocity and density statistics using spectral line data cubes. The VCA has been successfully tested using data cubes obtained via compressible magnetohydrodynamic simulations and has been applied to Galactic and Small Magellanic Cloud atomic hydrogen (HI) data [87,84,159,28]. Furthermore, the inclusion of absorption effects [85] has increased the power of this technique. Finally, the VCA can be applied to different species (CO, H α etc.) which should further increase its utility in the future.

Within the present discussion a number of results obtained with the VCA are important. First of all, the Small Magellanic Cloud (SMC) HI data exhibit a Kolmogorov-type spectrum for velocity and HI density from the smallest resolvable scale of 40 pc to the scale of the SMC itself, i.e. 4 kpc. Similar conclusions can be inferred from the Galactic data [52] for scales of dozens of parsecs, although the analysis has not been done systematically. Deshpande et al. [28] studied absorption of HI on small scales toward Cas A and Cygnus A. Within the VCA their results can be interpreted as implying that on scales less than 1 pc the HI velocity is suppressed by ambipolar drag and the spectrum of density fluctuations is shallow $P(k) \sim k^{-2.8}$. Such a spectrum [27] can account for the small scale structure of HI observed in absorption.

2.4 Magnetic field statistics

Magnetic field statistics are the most poorly constrained aspect of ISM turbulence. The polarization of starlight and of the Far-Infrared Radiation (FIR) from aligned dust grains is affected by the ambient magnetic fields. Assuming that dust grains are always aligned with their longer axes perpendicular to magnetic field (see the review [80]), one gets the 2D distribution of the magnetic field directions in the sky. Note that the alignment is a highly non-linear process in terms of the magnetic field and therefore the magnetic field strength is not available⁶.

The statistics of starlight polarization (see [40]) is rather rich for the Galactic plane and it allows to establish the spectrum⁷ $E(K) \sim K^{-1.5}$, where K is a two dimensional wave vector describing the fluctuations over sky patch.⁸

For uniformly sampled turbulence it follows from Lazarian & Shutenkov [83] that $E(K) \sim K^\alpha$ for $K < K_0$ and K^{-1} for $K > K_0$, where K_0^{-1} is the critical angular size of fluctuations which is proportional to the ratio of the injection energy scale to the size of the turbulent system along the line of sight. For Kolmogorov turbulence $\alpha = -11/3$.

However, the real observations do not uniformly sample turbulence. Many more close stars are present compared to the distant ones. Thus the intermediate slopes are expected. Indeed, Cho & Lazarian [22] showed through direct simulations that the slope obtained in [40] is compatible with the underlying Kolmogorov turbulence. At the moment FIR polarimetry does not provide maps that are really suitable to study turbulence statistics. This should change soon when polarimetry becomes possible using the airborne SOFIA observatory. A better understanding of grain alignment (see [80]) is required to interpret the molecular cloud magnetic data where some of the dust is known not to be aligned (see [82] and references therein).

Another way to get magnetic field statistics is to use synchrotron emission. Both polarization and intensity data can be used. The angular correlation of polarization data [3] shows the power-law spectrum $K^{-1.8}$ and we believe that the interpretation of it is similar to that of starlight polarization. Indeed, Faraday depolarization limits the depth of the sampled region. The intensity fluctuations were studied in [83] with rather poor initial data and the results were inconclusive. Cho & Lazarian [22] interpreted the fluctuations of synchrotron emissivity [43,44] in terms of turbulence with Kolmogorov spectrum.

⁶ The exception to this may be the alignment of small grains which can be revealed by microwave and UV polarimetry [80].

⁷ Earlier papers dealt with much poorer samples (see [65]) and they did not reveal power-law spectra.

⁸ This spectrum is obtained by [40] in terms of the expansion over the spherical harmonic basis Y_{lm} . For sufficiently small areas of the sky analyzed the multipole analysis results coincide with the Fourier analysis.

3 Theoretical Approaches to MHD Turbulence

Here we consider mainly Kolmogorov-type theories. Other theories not discussed in this section include the eddy-damped quasinormal Markovian (EDQNM) approximation [139], the renormalization group technique [39,174], and the direct interaction approximation [70].

3.1 Iroshnikov-Kraichnan theory

Attempts to describe magnetic turbulence statistics were made by Iroshnikov [61] and Kraichnan [71]. Their model of turbulence (IK theory) is isotropic in spite of the presence of the magnetic field.

We can understand the IK theory as follows.⁹ For simplicity, let us suppose that a uniform external magnetic field (\mathbf{B}_0) is present. In the incompressible limit, any magnetic perturbation propagates *along* the magnetic field line. To the first order, the speed of propagation is constant and equal to the Alfvén speed $V_A = B_0/\sqrt{4\pi\rho}$, where ρ is the density. Since wave packets are moving along the magnetic field line, there are two possible directions for propagation. If all the wave packets are moving in one direction, then they are stable to nonlinear order [132]. Therefore, in order to initiate turbulence, there must be opposite-traveling wave packets and the energy cascade occurs only when they collide. The IK theory starts from this observation.

The IK theory assumes that, when two opposite-traveling wave packets of size l collide, they lose the following amount of energy to smaller scales:

$$\Delta E \sim (dv^2/dt)\Delta t \sim \mathbf{v}_l \cdot \dot{\mathbf{v}}_l \Delta t \sim v_l(v_l^2/l)\Delta t \sim (v_l^3/l)(l/V_A), \quad (4)$$

where the IK theory assumes that only collisions between similar size packets are important and $\Delta t \sim l/V_A$. The latter means that the duration of the collision is the size of the wave packet divided by the speed of the wave packets. These assumptions look reasonable at first. But, it is important to note that they fail when eddies are anisotropic. That is, if eddies are elongated along the magnetic field line, then Δt is not l/V_A , but l_{\parallel}/V_A , where l_{\parallel} is the parallel size of the wave packet (or ‘eddy’).

Equation (4) tells us that the energy change per collision is $v_l^2(v_l/V_A)$, which is only a tiny fraction of v_l^2 when $V_A \gg v_l$. Therefore, in order for the eddy to transfer all the energy to small eddies, the eddy must go through many collisions. When such collisions are incoherent, we require a total $(v^2/\Delta E)^2$ collisions to complete the cascade. This means that the energy cascade time t_{cas} is

$$t_{cas} \sim \left(\frac{v^2}{\Delta E} \right)^2 \Delta t \sim \frac{l}{v_l} \frac{V_A}{v_l}, \quad (5)$$

which means that this new cascade time is (V_A/v_l) times longer than the eddy turnover time (l/v_l) . As in the Kolmogorov theory, the IK theory assumes the

⁹ We follow arguments in [46].

constancy of energy cascade (eq. 1): $(v_l^4)/(lV_A) = \text{constant}$, which, in turn, yields $v_l \propto l^{1/4}$, or,

$$\text{Iroshnikov-Kraichnan: } E(k) \propto k^{-3/2}. \quad (6)$$

3.2 Anisotropy

A uniform component to the magnetic field defines a special direction, which will be reflected in the dynamics of turbulent fluctuations. One obvious effect is that it is easy to mix field lines in directions perpendicular to the local mean magnetic field and much more difficult to bend them. The IK theory assumes isotropy of the energy cascade in Fourier space, an assumption which has attracted severe criticism [115,153,114,158,104]. Mathematically, anisotropy manifests itself in the resonant conditions for 3-wave interactions:

$$\mathbf{k}_1 + \mathbf{k}_2 = \mathbf{k}_3, \quad (7)$$

$$\omega_1 + \omega_2 = \omega_3, \quad (8)$$

where \mathbf{k} 's are wavevectors and ω 's are wave frequencies. The first condition is a statement of wave momentum conservation and the second is a statement of energy conservation. Alfvén waves satisfy the dispersion relation: $\omega = V_A |k_{\parallel}|$, where k_{\parallel} is the component of wavevector parallel to the background magnetic field. Since only opposite-traveling wave packets interact, \mathbf{k}_1 and \mathbf{k}_2 must have opposite signs. Then from equations (7) and (8), either $k_{\parallel,1}$ or $k_{\parallel,2}$ must be equal to 0 and $k_{\parallel,3}$ must be equal to the nonzero initial parallel wavenumber. That is, zero frequency modes are essential for energy transfer [153]. Therefore, in the wavevector space, 3-wave interactions produce an energy cascade which is strictly perpendicular to the mean magnetic field. However, in real turbulence, equation (8) does not need to be satisfied exactly, but only to within an error of order $\delta\omega \sim 1/t_{cas}$ [45]. This implies that the energy cascade is not strictly perpendicular to \mathbf{B}_0 , although clearly very anisotropic.

It is noteworthy that there has been a claim that “by increasing the magnitude of the mean field in 3-D simulations one finds that the transition from the isotropic 3-D scaling properties toward those observed in 2-D” [6]. (see also [7,175,6] for recent development in 2-D MHD turbulence). This claim has yet to be substantiated, however. We feel that the available numerical simulations [116,20,101] are reasonably consistent with the Goldreich & Sridhar [45] model that we review in the next section. It is also worth noting that the idea of an anisotropic (perpendicular) cascade has been incorporated into the framework of the reduced MHD approximation [161,146,113,182,4].

3.3 Goldreich-Sridhar theory

We assume throughout this discussion that the rms turbulent velocity at the energy injection scale is comparable to the Alfvén speed of the mean field and consider only scales below the energy injection scale. Consequently, we are not

concerned with the problem of magnetic field generation, or the magnetic dynamo which is considered elsewhere in this volume (see also [111,132,72] for reviews, [107,123,12,15] for numerical calculations, [173,53,15] for suppression of the α dynamo effect in highly conducting fluids, and [73,11,176,100,185] for recent developments).

An ingenious model very similar in its beauty and simplicity to the Kolmogorov model has been proposed by Goldreich & Sridhar [45] (1995; hereinafter GS95) for incompressible MHD turbulence. They pointed out that motions perpendicular to the magnetic field lines mix them on a hydrodynamic time scale, i.e. at a rate $t_{cas}^{-1} \approx k_{\perp} v_l$, where k_{\perp} is the wavevector component perpendicular to the local mean magnetic field and $l \sim k^{-1} (\approx k_{\perp}^{-1})$. These mixing motions couple to the wave-like motions parallel to magnetic field giving a *critical balance* condition

$$k_{\parallel} V_A \sim k_{\perp} v_k, \quad (9)$$

where k_{\parallel} is the component of the wavevector parallel to the local magnetic field. When the typical k_{\parallel} on a scale k_{\perp} falls below this limit, the magnetic field tension is too weak to affect the dynamics and the turbulence evolves hydrodynamically, in the direction of increasing isotropy in phase space. This quickly raises the value of k_{\parallel} . In the opposite limit, when k_{\parallel} is large, the magnetic field tension dominates, the error $\delta\omega$ in the matching conditions is reduced, and the nonlinear cascade is largely in the k_{\perp} direction, which restores the critical balance.

If conservation of energy in the turbulent cascade applies locally in phase space then the energy cascade rate (v_l^2/t_{cas}) is constant (eq. 1): $(v_l^2)/(l/v_l) = \text{constant}$. Combining this with the critical balance condition we obtain an anisotropy that increases with decreasing scale

$$k_{\parallel} \propto k_{\perp}^{2/3}, \quad (10)$$

and a Kolmogorov-like spectrum for perpendicular motions

$$v_l \propto l^{1/3}, \quad \text{or, } E(k) \propto k_{\perp}^{-5/3}, \quad (11)$$

which is not surprising since the magnetic field does not influence motions that do not bend it. At the same time, the scale-dependent anisotropy reflects the fact that it is more difficult for the weaker, smaller eddies to bend the magnetic field.

GS95 shows the duality of motions in MHD turbulence. Those perpendicular to the mean magnetic field are essentially eddies, while those parallel to magnetic field are waves. The critical balance condition couples these two types of motions.

3.4 Weak/Intermediate turbulence.

Let us reconsider the interaction of two wave packets moving oppositely along the mean magnetic field line. As in equation (4), the energy loss per collision is

$$\Delta E \sim (v^2)\Delta t \sim (v_l^3/l_{\perp})(l_{\parallel}/V_A), \quad (12)$$

where we explicitly distinguish the parallel (l_{\parallel}) and the perpendicular size (l_{\perp}). The kinetic energy of the eddy is v_l^2 . Therefore, the ratio of ΔE to E ,

$$\zeta_l \equiv \frac{\Delta E}{v_l^2} \sim \frac{v_l l_{\parallel}}{V_A l_{\perp}} = \frac{v_l k_{\perp}}{V_A k_{\parallel}}, \quad (13)$$

characterizes the strength of the nonlinear interaction [45]. In the GS95 theory, $\zeta_l \sim 1$. This means that $V_A \approx V$ is required at the energy injection scale when energy injection is isotropic ($k_{\perp,L} \sim k_{\parallel,L}$). When this condition is satisfied, the turbulence is called *strong* turbulence.

There are some astrophysical situations, e.g. the Jovian magnetosphere [148], where the parameter ζ_L is much smaller than the unity over a broad range of length scales. Although as noted above the cascade will evolve in the direction of increasing ζ_l for decreasing l , and may reach the strong turbulent regime on very small scales. In this regime, the parallel cascade is strongly suppressed so the turbulence is qualitatively different from the strong turbulence discussed above. This is the *weak* turbulence regime. We do not discuss this type of turbulence here due to its limited astrophysical applicability and restricted inertial range. For more information, see [129,158,122,46,42]. Note that Galtier et al. [42] obtained $E(k) \sim k_{\perp}^{-2}$ (see also [46]).

4 Testing and Extending Incompressible Theory

Here we focus on recent direct numerical simulations related to the anisotropic structure of MHD turbulence. A discussion of earlier pioneering numerical simulations of MHD turbulence can be found in [140,107].

4.1 Scaling laws

Despite its attractiveness, the Goldreich-Sridhar model is a conjecture that requires testing. The first such test was done by Cho & Vishniac [20] who used an incompressible pseudo-spectral MHD code with 256^3 grid points. In their simulations, they used $V_A = B_0/\sqrt{4\pi\rho} \sim V$. Their results for eddy shapes are shown in Figure 4a, which shows a reasonable agreement with the predicted scale-dependent anisotropy of the turbulence (eq. (10)) in the inertial range (i.e. the scales between the energy injection scale and the dissipation scale). They also obtained $E(k) \sim k^{-5/3}$ in the inertial range. Yet although the velocity does show the expected scaling, the magnetic field scaling is a bit more uncertain.

A subsequent numerical study by Maron & Goldreich [101] performed with a different code and in a different physical regime, namely, for $V_A \gg V$, also supported the GS95 model and clarified the role of pseudo-Alfvén and Alfvén modes. In particular, they confirmed that the pseudo-Alfvén modes are passively carried down the cascade through interactions with the Alfvén modes. They also showed that passive scalars adopt the same power spectrum as the velocity and magnetic field fluctuations. In addition, they addressed several issues about the

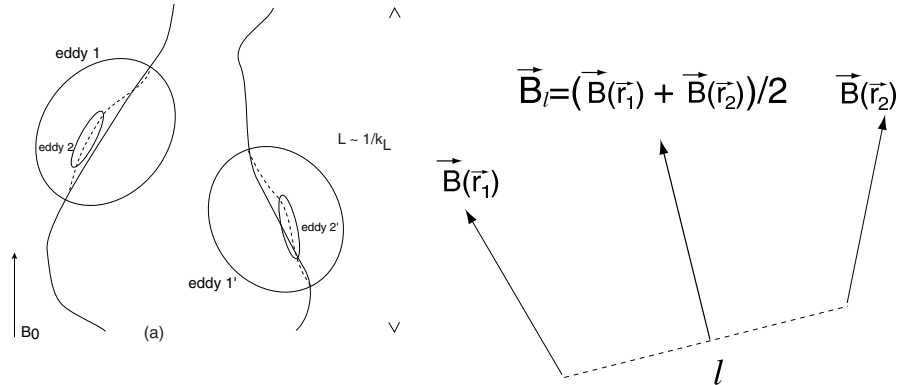


Fig. 1. (a) Eddies and local mean magnetic field. Local mean field is the properly averaged magnetic field near eddies under consideration. Eddies at different locations (e.g. eddies 1 & 1') can have different local mean fields. Eddies of different sizes (e.g. eddies 1 & 2) can also have different local mean fields. When we do not take into account the local mean field, calculations hardly reveal true eddy structures. From [23]. (b) An example of calculating the local mean field. The direction of the local mean field \mathbf{B}_l is obtained by the pair-wise average: $\mathbf{B}_l = (\mathbf{B}(\mathbf{r}_1) + \mathbf{B}(\mathbf{r}_2))/2$.

imbalanced cascade. Overall, they obtained results reasonably consistent with the GS95 model, but their energy spectra scale slightly differently: $E(k) \propto k^{-3/2}$. They attributed this result to intermittency.

Müller & Biskamp [116] studied MHD turbulence numerically in the regime of $V \gg V_A$ and obtained a Kolmogorov spectrum: $E(k) \sim k^{-5/3}$. They numerically studied the scaling exponents and obtained $\zeta_2 \approx 0.7$ and $\zeta_3 \approx 1$ (see the definition of the scaling exponents in the next subsection). The value of ζ_2 is consistent with the energy spectrum.

Other related recent numerical simulations include Matthaeus et al. [104] and Milano et al. [109]. Matthaeus et al. [104] showed that the anisotropy of low frequency MHD turbulence scales linearly with the ratio of perturbed and total magnetic field strength b/B ($= b/(b^2 + B_0^2)^{1/2}$).¹⁰

¹⁰ In fact we can derive the GS95 scaling using this result. Although their analysis was based on comparing the strength of a uniform background field and the magnetic perturbations on all scales, we can reinterpret this result by assuming that the strength of random magnetic field at a scale l is b_l , and that the background field is the sum of all contributions from larger scales. Then Matthaeus et al.'s result becomes a prediction that the anisotropy (k_{\parallel}/k_{\perp}) is proportional to (b_l/B) . We can take the total magnetic field strength $B \sim \text{constant}$ as long as the background field is stronger than the perturbations on all scales. Since $b_l \sim (kE(k))^{1/2} \sim k_{\perp}^{-1/3}$, we obtain an anisotropy (k_{\parallel}/k_{\perp}) proportional to $k_{\perp}^{-1/3}$, and $k_{\parallel} \propto k_{\perp}^{2/3}$. In this interpretation, smaller eddies are more elongated because they have a smaller b_l/B ratio.

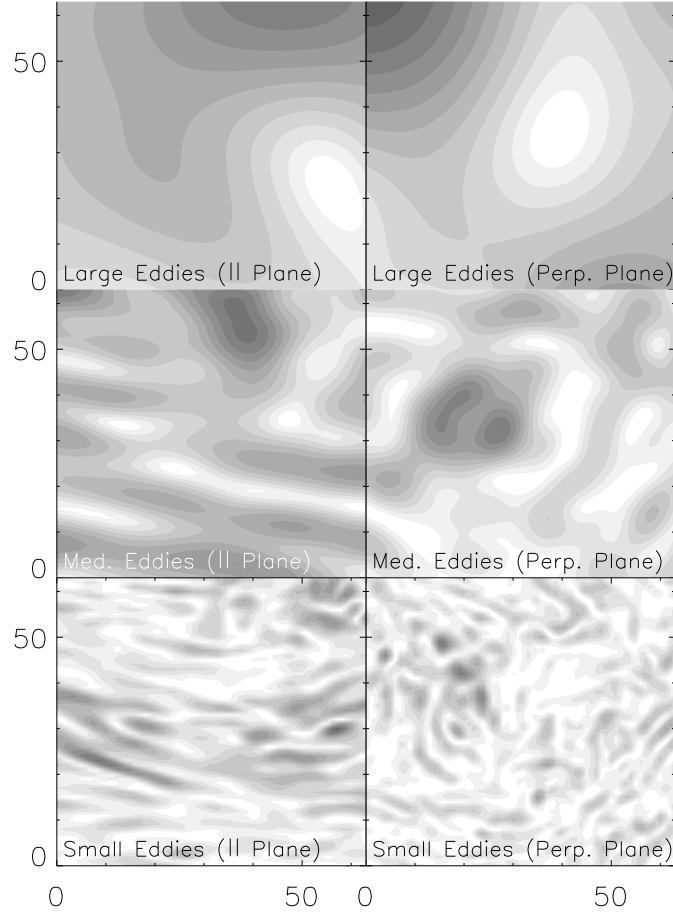


Fig. 2. Cross-sections of the data cube. (*Left panels*) $|\mathbf{b}_l|$ in a plane \parallel to \mathbf{B}_0 . (*Right panels*) $|\mathbf{b}_l|$ in a plane \perp to \mathbf{B}_0 . In the left panels, \mathbf{B}_0 is along the horizontal axis. *Large scale eddies* are obtained from the Fourier components with $1 \leq k < 4$. *Medium scale eddies* are obtained from the Fourier components with $4 \leq k < 16$. *Small scale eddies* are obtained from the Fourier components with $16 \leq k < 64$. The small scale eddies show a high degree of elongation in the parallel plane. However, they do not show a systematic behavior in the perpendicular plane.

All in all, numerical simulations so far have been largely, but not perfectly, consistent with the GS95 theory, e.g. the Kolmogorov-type scaling and the scale-dependent anisotropy ($k_{\parallel} \propto k_{\perp}^{2/3}$), and helped to extend it. An important point, which was not included in some of the earlier work, is that the scale dependent anisotropy can be measured only in a local coordinate frame which is aligned with the *locally averaged* magnetic field direction [20]. The necessity of using a local frame is due to the fact that eddies are aligned along the local mean magnetic fields, rather than the global mean field \mathbf{B}_0 . Since smaller scale eddies

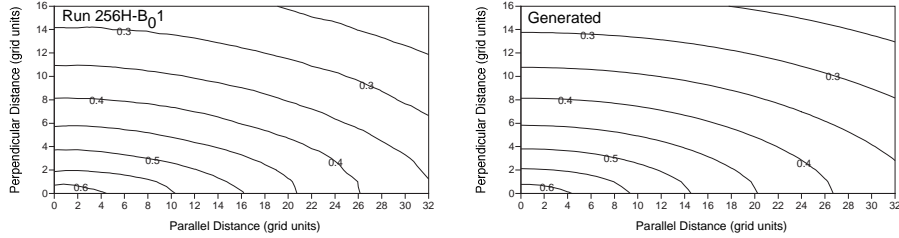


Fig. 3. (a) Velocity correlation function (VCF) from a simulation. The contours represent shape of different size eddies. The smaller contours (or, eddies) are more elongated. (b) VCF generated from equation (14). From [23].

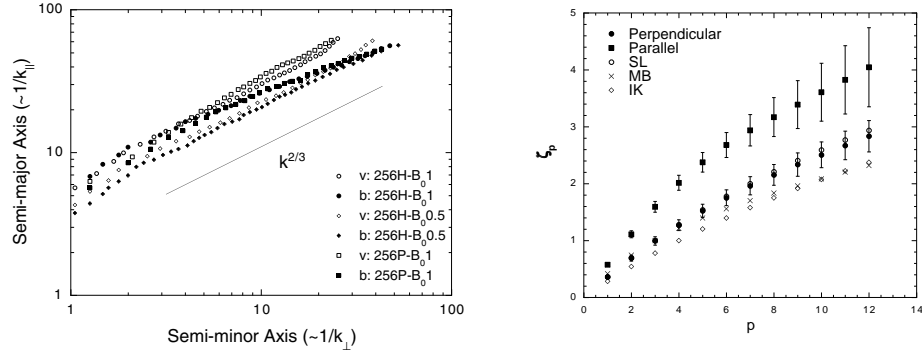


Fig. 4. (a) Semi-major axis and semi-minor axis of contours of the VCF shown in Figure 3a. The results support $k_{\parallel} \propto k_{\perp}^{2/3}$. From [20]. (b) Scaling exponents. From [23].

are weaker, and more anisotropic, measurements of eddy shape based on a global coordinate system are always dominated by the largest eddies in the simulation. Figure 1 illustrates the concept of a local frame and one way to identify it. Further research in Cho, Lazarian, & Vishniac [23] (2002a: hereinafter CLV02a) showed that in the local system of reference the mixing motions perpendicular to the magnetic field have statistics identical to hydrodynamic turbulence (cf. Müller & Biskamp [116]).

Fig. 2 shows the shapes of eddies of different sizes. Left panels show an increased anisotropy as we move from the top (large eddies) to the bottom (small eddies). The horizontal axes of the left panels are parallel to \mathbf{B}_0 . Structures in the perpendicular plane do not show a systematic elongation.

Fig. 3a and Fig. 4a quantify some of these results. The contours of the correlation function obtained in [20] are shown in Fig. 3a and are consistent with the predictions of the GS95 model. Fig. 4a shows that the semi-major axis ($1/k_{\parallel}$) is proportional to the 2/3 power of the semi-minor axis ($1/k_{\perp}$), implying that $k_{\parallel} \propto k_{\perp}^{2/3}$. While the one dimensional energy spectrum follows Kolmogorov spec-

trum, $E(k) \propto k^{-5/3}$, CLV02a showed that the 3D energy spectrum can be fit by

$$P(k_{\perp}, k_{\parallel}) = (B_0/L^{1/3})k_{\perp}^{-10/3} \exp\left(-L^{1/3} \frac{k_{\parallel}}{k_{\perp}^{2/3}}\right), \quad (14)$$

where B_0 is the strength of the mean field and L is the scale of energy injection. The velocity correlation from the 3D spectrum provides an excellent fit to the numerical data (Fig. 3b). This allows practical applications illustrated in §5.

4.2 Intermittency

Intermittency refers to the non-uniform distribution of dissipative structures. Intermittency has an important dynamical consequence: it affects the energy spectrum. Highly intermittent turbulent structures were invoked by Falgarone et al. [37] and Joulain et al. [63] as the primary location of endothermic interstellar chemical reactions.

Maron & Goldreich [101] studied the intermittency of dissipation structures in MHD turbulence using the fourth order moments of the Elsasser fields and the gradients of the fields. Their simulations show strong intermittent structures. CLV02a used a different, but complementary, method to study intermittency, based on the higher order longitudinal structure functions. They found that by this measure the intermittency of velocity field in MHD turbulence across local magnetic field lines is as strong as, but not stronger than, hydrodynamic turbulence.

In fully developed hydrodynamic turbulence, the (longitudinal) velocity structure functions $S_p = \langle ([\mathbf{v}(\mathbf{x} + \mathbf{r}) - \mathbf{v}(\mathbf{x})] \cdot \hat{\mathbf{r}})^p \rangle \equiv \langle \delta v_L^p(\mathbf{r}) \rangle$ are expected to scale as r^{ζ_p} . For example, the classical Kolmogorov phenomenology (K41) predicts $\zeta_p = p/3$. The (exact) result for $p=3$ is the well-known 4/5-relation: $\langle \delta v_L^3(\mathbf{r}) \rangle = -(4/5)\epsilon r$, where ϵ is the energy injection rate (or, energy dissipation rate) (see e.g. [41]). On the other hand, considering intermittency, She & Leveque ([152]; hereinafter S-L) proposed a different scaling relation: $\zeta_p^{SL} = p/9 + 2[1 - (2/3)^{p/3}]$. Note that the She-Leveque model also implies $\zeta_3 = 1$.

So far in MHD turbulence, to the best of our knowledge, there is no rigorous intermittency theory which takes into account scale-dependent anisotropy. Politano & Pouquet [135] have developed an MHD version of the She-Leveque model:

$$\zeta_p^{PP} = \frac{p}{g}(1-x) + C \left(1 - (1-x/C)^{p/g}\right), \quad (15)$$

where C is the co-dimension of the dissipative structure, g is related to the scaling $v_l \sim l^{1/g}$, and x can be interpreted as the exponent of the cascade time $t_{cas} \propto l^x$. (In fact, g is related to the scaling of Elsasser variable $z=v \pm b$: $z_l \sim l^{1/g}$.) In the framework of the IK theory, where $g = 4$, $x = 1/2$, and $C = 1$ when the dissipation structures are sheet-like, their model of intermittency becomes $\zeta_p^{IK} = p/8 + 1 - (1/2)^{p/4}$. On the other hand, Müller & Biskamp [116]

performed numerical simulations on decaying isotropic MHD turbulence and obtained Kolmogorov-like scaling ($E(k) \sim k^{-5/3}$ and $t \sim l^{2/3}$) and sheet-like dissipation structures, which implies $g = 3$, $C = 1$, and $x = 2/3$. From equation (15), they proposed that

$$\zeta_p^{MB} = p/9 + 1 - (1/3)^{p/3}. \quad (16)$$

The intermittency results from [23] are shown in Fig. 4b. The filled circles represent the scaling exponents of longitudinal velocity structure functions in directions *perpendicular* to the local mean magnetic field. It is surprising that the scaling exponents are so close to the original (i.e. hydrodynamic) S-L model. This raises an interesting question. In the simulations of CLV02a, $t_{cas} \propto l^{2/3}$ and $E(k) \propto k^{-5/3}$ scaling is observed. It is observed that MHD turbulence has sheet-like dissipation structures [137]. Therefore, the parameters for CLV02a simulations should be the same as those of Müller & Biskamp's (i.e. $g = 3$, $C = 1$, and $x = 2/3$) rather than suggesting $C = 2$. We believe this difference stems from the different simulation settings (Müller & Biskamp's turbulence is isotropic and CLV02a's is anisotropic) and the way the turbulence is analyzed (global versus local frame). In fact, we expect the the small scale behavior of MHD turbulence should not depend on whether the largest scale fields are uniform or have the same scale of organization as the largest turbulent eddies. Nevertheless, given the limited dynamical range available in these simulations, it would not be surprising if the scale of the magnetic field has an impact on the intermittency statistics. It is not clear how scale-dependent anisotropy changes the intermittency model in equation (15) and we will not discuss this issue further. Instead, we simply stress that a striking similarity exists between ordinary hydrodynamic turbulence and MHD turbulence in perpendicular directions, which further supports the picture of the GS95 turbulence.¹¹

In Figure 5a, we also plot the scaling exponents (represented by filled squares) of longitudinal velocity structure functions *along* directions of the local mean magnetic field. Although we show only the exponents of longitudinal structure functions, those of transverse structure functions follow a similar scaling law. Evidently intermittency along the local mean magnetic field directions is completely different from the scaling predicted by previous (isotropic) models. Roughly speaking, the scaling exponents along the directions of local magnetic field are 1.5 times larger than those of perpendicular directions. This has an obvious similarity to the scaling of eddy shapes.

The second order exponent ζ_2 is related to the the 1-D energy spectra: $E(k_\perp) \propto k_\perp^{-(1+\zeta_2)}$. Previous 2-D driven MHD calculations for $B_0 = 0$ by Politano, Pouquet, & Carbone [136] also found $\zeta_2 \sim 0.7$. However, Biskamp, & Schwarz [7] obtained $\zeta_2 \sim 0.5$ from decaying 2-D MHD calculations with $B_0 = 0$. The result of CLV02a suggests that ζ_2 is closer to $2/3$, rather than to $1/2$. (It is not clear whether or not the scaling exponents follow the original S-L model exactly. At the same time, our calculation shows that the original S-L model can

¹¹ MG01 attributed the deviation of their spectrum from the Kolmogorov-type to the intermittency present in their simulation.

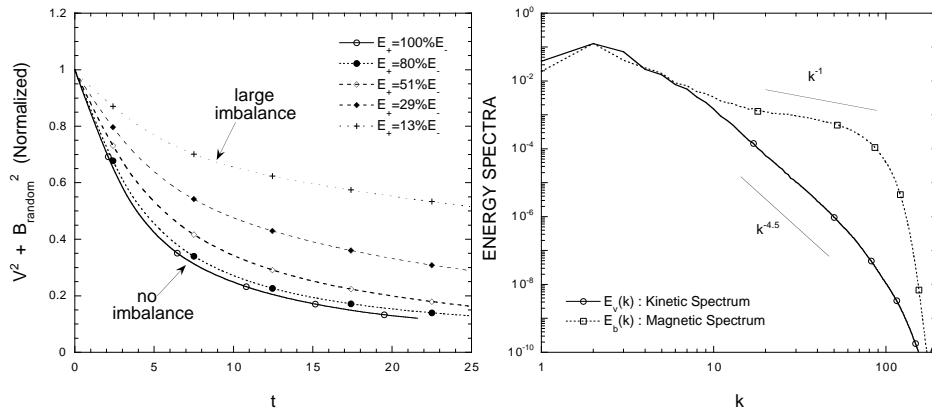


Fig. 5. (a) *(Left)* Imbalanced Decay. When imbalance is large, turbulence decays slow. From CLV02a. (b) *(Right)* Viscous damped regime. A new inertial range emerges below the viscous cut-off at $k \sim 7$. From Cho, Lazarian, & Vishniac (2002b).

be a good approximation for our scaling exponents. The S-L model predicts that ($\zeta_2 \sim 0.696$.) This is equivalent to our earlier claim that our result supports the scaling law $E(k_{\perp}) \propto k_{\perp}^{-5/3}$ at least for velocity. For the parallel directions, the results support $E(k_{\parallel}) \propto k_{\parallel}^{-2}$ although the uncertainty is large.

5 Damping of Turbulence

5.1 Imbalanced cascade

Turbulence plays a critical role in molecular cloud support and star formation and the issue of the time scale of turbulent decay is vital for understanding these processes. If MHD turbulence decays quickly, then serious problems face the researchers attempting to explain important observational facts, e.g. turbulent motions seen within molecular clouds without star formation [119] and rates of star formation [106]. Earlier studies attributed the rapid decay of turbulence to compressibility effects [99]. GS95 predicts and numerical simulations, e.g. CLV02a, confirm that MHD turbulence decays rapidly even in the incompressible limit. This can be understood if mixing motions perpendicular to magnetic field lines are considered. As we discussed earlier, such eddies, as in hydrodynamic turbulence, decay in one eddy turnover time.

Below we consider the effect of imbalance [103,165,50,60,101] on the turbulence decay time scale. Duality of the MHD turbulence means that the turbulence can be described by colliding wave packets. ‘Imbalance’ means that the flux of wave packets traveling in one direction is significantly larger than those traveling in the other direction. In the ISM, many energy sources are localized both in space and time. For example, in terms of energy injection, stellar outflows are essentially point energy sources. With these localized energy sources, it is natural that interstellar turbulence be typically imbalanced.

Here we show results of the CLV02a study that demonstrate that imbalance does extend the lifetime of MHD turbulence (Fig. 5a). We used a run on a grid of 144^3 to investigate the decay time scale. For initial conditions we took a data cube from a driven turbulence simulation. The initial data cube contains both upward (denoted as $+$) and downward moving waves (denoted as $-$). To adjust the degree of initial imbalance, we either increased or decreased the energy of the upward moving components and, by turning off the forcing terms, let the turbulence decay. Note that the initial energy is normalized to 1. The y-axis is the normalized total (=up + down) energy.

The dependence of the turbulence decay time on the degree of imbalance is an important finding. To what degree the results persist in the presence of compressibility is the subject of our current research. It is obvious that results of CLV02a are applicable to incompressible, namely, Alfvén motions.¹² We show in §6.3 that the Alfvén motions are essentially decoupled from compressible modes. As the result we expect that the turbulence decay time may be substantially longer than one eddy turnover time provided that the turbulence is imbalanced.

5.2 Ion-neutral damping: a new regime of turbulence

In hydrodynamic turbulence viscosity sets a minimal scale for motion, with an exponential suppression of motion on smaller scales. Below the viscous cutoff the kinetic energy contained in a wavenumber band is dissipated at that scale, instead of being transferred to smaller scales. This means the end of the hydrodynamic cascade, but in MHD turbulence this is not the end of magnetic structure evolution. For viscosity much larger than resistivity, $\nu \gg \eta$, there will be a broad range of scales where viscosity is important but resistivity is not. On these scales magnetic field structures will be created by the shear from non-damped turbulent motions, which amounts essentially to the shear from the smallest undamped scales. The created magnetic structures would evolve through generating small scale motions. As a result, we expect a power-law tail in the energy distribution, rather than an exponential cutoff. To our best knowledge, this is a completely new regime for MHD turbulence.

In partially ionized gas neutrals produce viscous damping of turbulent motions. In the Cold Neutral Medium (see Draine & Lazarian [34] for a list of the idealized phases) this produces damping on the scale of a fraction of a parsec. The magnetic diffusion in those circumstances is still negligible and exerts an influence only at the much smaller scales, $\sim 100km$. Therefore, there is a large range of scales where the physics of the turbulent cascade is very different from the GS95 picture.

¹² In the long run, the imbalance will be defeated by the parametric instability, which develops through formation of density inhomogeneities within the beam of Alfvén waves [26,47,62,25]. However, this instability takes many wave periods to be established. A similar argument can be applied when we consider completely imbalanced cascade. That is, even in the completely imbalanced cascade decay of energy can occur due to non-linear steepening if waves. But, this will be very slow for Alfvén waves.

Cho, Lazarian, & Vishniac [24] have explored this regime numerically. Here we used a grid of 384^3 and a physical viscosity for velocity damping. The kinetic Reynolds number is around 100. With this Reynolds number, viscous damping occurs around $k \sim 7$, or about $\sim 1/7$ of the width of the computational box. We minimized magnetic diffusion through the use of a hyper-diffusion term of order 3. To test for possible “bottle neck” effects we also did simulations with normal magnetic diffusion and reproduced similar results but only over a reduced dynamical range. The bottleneck effect is a common feature in numerical hydrodynamic simulations with hyperviscosity. See [8] for MHD simulations.

In Fig. 5b, we plot energy spectra. The spectra consist of several parts. First, the peak of the spectra corresponds to the energy injection scale. Second, for $2 < k < 7$, kinetic and magnetic spectra follow a similar slope. This part is more or less a severely truncated inertial range for undamped MHD turbulence. Third, the magnetic and kinetic spectra begin to decouple at $k \sim 7$. Fourth, after $k \sim 20$, a new *damped-scale inertial range* emerges. In the new inertial range, magnetic energy spectrum follows

$$\text{New Regime: } E_b(k) \propto k^{-1}, \quad (17)$$

implying considerable magnetic structures below the viscous damping scale. The velocity power spectrum steepens in this regime, but does not fall exponentially.

Figure 6a shows that the small magnetic structures are highly intermittent in the viscous-damped regime. Here we obtained the small scale magnetic field by eliminating Fourier modes with $k < 20$. We can see that the typical radius of curvature of field lines in the plane is much larger than the typical perpendicular scale for field reversal. The typical radius of curvature of field lines corresponds to the viscous damping scale, indicating that stretched structures are results of the shearing motions at the viscous damping scale. There is no preferred direction for these elongated structures. A similar plot for ordinary (*not* viscously damped) MHD turbulence (Fig. 6b) shows much less intermittent structures. We remove Fourier modes with $k < 20$ also in Fig. 6b.

A theoretical model for this new regime and its consequences for stochastic reconnection [89] will be found in an upcoming paper (Lazarian, Vishniac, & Cho 2002). Here we summarize the main points of the model. We begin by noting that the strong intermittency seen in this regime suggests a new parameter, f_l , which is the volume filling fraction of structures with scales comparable to l . This in turn implies that we need to distinguish between volume averaged means and typical values of velocity and magnetic field perturbations in fraction of space where they are concentrated. We denote the latter with a ‘^’, so that $v_l^2 = f_l \hat{v}_l^2$, and $b_l^2 = f_l \hat{b}_l^2$. This model does not include information about the range of field strengths or velocities with structure on a scale l in the bulk of the volume, aside from assuming that they are sufficiently weak that they do not contribute to any global averages.

The second new fundamental parameter in this model is the eddy turn over rate at the damping scale, k_d , i.e.

$$\tau_s^{-1} \sim k_d v_d \sim k_d^2 \nu_n, \quad (18)$$

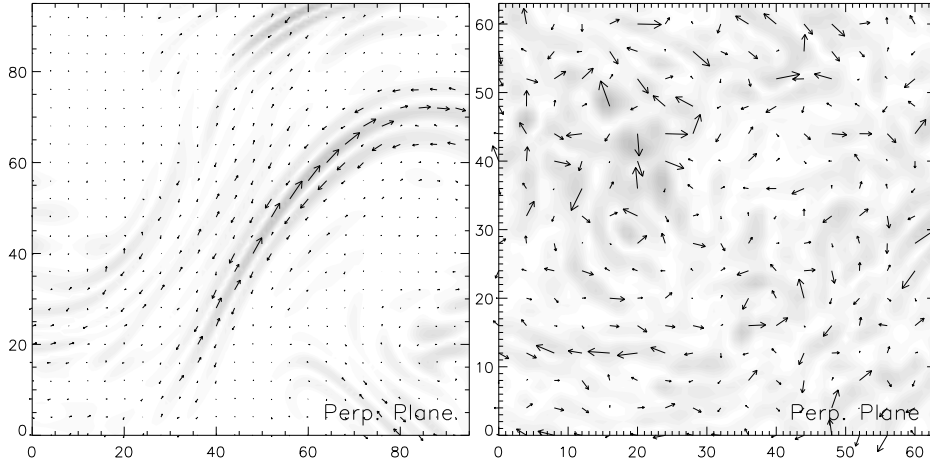


Fig. 6. (*Left*) Viscous-damped turbulence. Strength of magnetic field in a plane perpendicular to \mathbf{B}_0 . Arrows are magnetic fields in the plane. Only a part of the plane is shown. Note highly intermittent structures. From [24]. (*Right*) Same as *Left*, but for ordinary (not viscous-damped) MHD turbulence. Structures are less intermittent.

where v_d is the velocity at $l_d \sim 1/k_d$ and ν_n is the viscosity of the plasma due to neutral particles, which differs from the viscosity of neutral fluid by the ratio of atomic to total densities.

Since motions on smaller scales are strongly damped, the cascade of magnetic energy to smaller scales is due to motions on the damping scale. This implies that

$$b_l^2/\tau_s \sim \text{constant}, \quad (19)$$

so that b_l is maintained approximately at the level of magnetic field at the damping scale, b_d .

This folding and refolding, perpendicular to the mean field direction, has a weak effect on the field line curvature. (This result is also seen in the simulations.) The decrease in the structure length l is due to an increase in the magnetic field gradient perpendicular to the mean field direction. The resulting magnetic pressure gradients are balanced by plasma pressure gradients. Thus on the scales below the viscous cutoff, the tension forces are balanced by viscous drag, i.e.

$$\frac{\rho \nu_n}{l^2} \hat{v}_l \sim \max[k_d \hat{b}_l, k_{\parallel} B_0] \hat{b}_l. \quad (20)$$

Finally, this dynamic equilibrium can be maintained only if the small scale motions are strong enough to counteract the shear, τ_s^{-1} . In other words, $\hat{v}_l/l \sim \tau_s^{-1}$.

Combining these results we see that $f_l \sim k_d l$, $\hat{b}_l \sim b_d (k_d l)^{-1/2}$, and $v_l \propto l^{3/2}$. These scaling laws are at least qualitatively consistent with the simulation results, although the velocity power spectrum may be slightly steeper than the model prediction.

Unfortunately, a realistic treatment of the ISM requires an explicit recognition of the two fluid nature of the partially ionized plasma, rather than simply representing neutral drag with an effective viscosity. Here we are beyond the reach of available simulations, and need to rely on an extension of the scaling arguments given above.

First, at sufficiently small values of l , the ambipolar diffusion time ($\sim k^2 t_{in} (b_l^2 / \rho_{tot}) (\rho_n / \rho_i)$, where t_{in} = ion-neutral collision time) will become less than τ_s , and the magnetic pressure gradients will be supported entirely by the ionized particle pressure. This means that only a fraction, $\sim \rho_i / \rho_{tot}$, of the energy will continue the cascade to smaller scales.

Next, for some ion-neutral collision time, t_{in} , there will be some decoupling scale, l_c , where

$$\rho \nu_n / l_c^2 \sim \rho_i / t_{in}. \quad (21)$$

At smaller scales the ions will be dragged through a more or less uniform neutral background. The argument above needs to be modified by replacing the viscous drag coefficient in equation (20) with the right hand side of equation (21). This gives

$$f_l \propto l^{-1}, \quad (22)$$

$$\hat{b}_l \propto l^{1/2}, \quad \text{and} \quad v_l \propto l^{1/2}. \quad (23)$$

Finally, at some sufficiently small scale the filling factor will rise to unity, and the gradients in the magnetic field will become strong enough that neutral drag can be ignored. These conditions are satisfied simultaneously when

$$k_d l \sim t_{in} / \tau_s. \quad (24)$$

Below this scale we expect to see a resumption of the turbulent cascade, now involving only the ionized component of the plasma, down to scales where plasma resistivity and viscosity finally dissipate the remaining energy. Since the longest cascade time for this regime is $t_{in} \ll \tau_s$, we expect this small scale turbulence to be intermittent, with a duty cycle $\sim t_{in} / \tau_s$.

All the consequences of the new regime of the MHD turbulence have not yet been appreciated, but we expect that it will have a substantial impact on our understanding of the interstellar physics. Moreover, the treatment given above actually applies only when ρ_i / ρ is not very small. Otherwise the decoupling scale can be larger than the viscous damping scale.

6 Compressible Turbulence

For the rest of the review, we consider MHD turbulence of a single conducting fluid. While the GS95 model describes incompressible MHD turbulence well, no universally accepted theory exists for compressible MHD turbulence despite various attempts (e.g., [56]). Earlier numerical simulations of compressible MHD turbulence covered a broad range of astrophysical problems, such as the decay of turbulence (e.g. [98,160]) or turbulent modeling of the ISM (see recent review

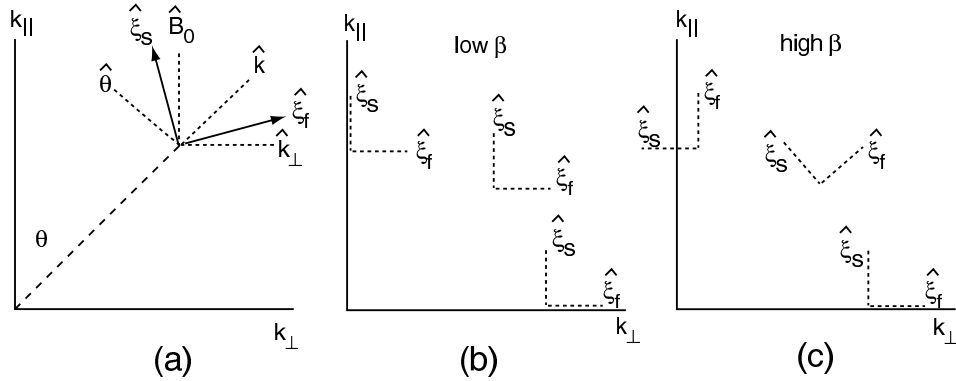


Fig. 7. (a) Directions of fast and slow basis vectors. $\hat{\xi}_f$ and $\hat{\xi}_s$ represent the directions of displacement of fast and slow modes, respectively. In the fast basis ($\hat{\xi}_f$) is always between $\hat{\mathbf{k}}$ and $\hat{\mathbf{k}}_{\perp}$. In the slow basis ($\hat{\xi}_s$) lies between $\hat{\theta}$ and $\hat{\mathbf{B}}_0$. Here, $\hat{\theta}$ is perpendicular to $\hat{\mathbf{k}}$ and parallel to the wave front. All vectors lie in the same plane formed by \mathbf{B}_0 and \mathbf{k} . On the other hand, the displacement vector for Alfvén waves (not shown) is perpendicular to the plane. (b) Directions of basis vectors for a very small β drawn in the same plane as in (a). The fast bases are almost parallel to $\hat{\mathbf{k}}_{\perp}$. (c) Directions of basis vectors for a very high β . The fast basis vectors are almost parallel to $\hat{\mathbf{k}}$. The slow waves become pseudo-Alfvén waves.

[170]; see also [133,168,134,169] for earlier 2D simulations and [125,126,131,67,9] for recent 3D simulations). In what follows, we concentrate on the fundamental properties of compressible MHD.

6.1 Alfvén, slow, and fast modes

Let us start by reviewing different MHD waves. In particular, we describe the Fourier space representation of these waves. The real space representation can be found in papers on modern shock-capturing MHD codes (e.g. [13,147]). For the sake of simplicity, we consider an isothermal plasma. Figure 7 and Figure 8

Table 1. Notations for compressible turbulence

Notation	Meaning
a, c_s, c_f, V_A	sound, slow, fast, and Alfvén speed
$\delta V, (\delta V)_s, (\delta V)_f, (\delta V)_A$	random (rms) velocity
	Previously we used V for the rms velocity
$v_l, (v_l)_s, (v_l)_f, (v_l)_A$	velocity at scale l
$\mathbf{v}_{\mathbf{k}}, (\mathbf{v}_{\mathbf{k}})_s, (\mathbf{v}_{\mathbf{k}})_f, (\mathbf{v}_{\mathbf{k}})_A$	velocity vector at wavevector \mathbf{k}
$\hat{\mathbf{B}}_0 (= \hat{\mathbf{k}}_{\parallel}), \hat{\mathbf{k}}_{\perp}, \hat{\mathbf{k}}, \hat{\theta}, \dots$	unit vectors
$\hat{\xi}_s, \hat{\xi}_f$	displacement vectors

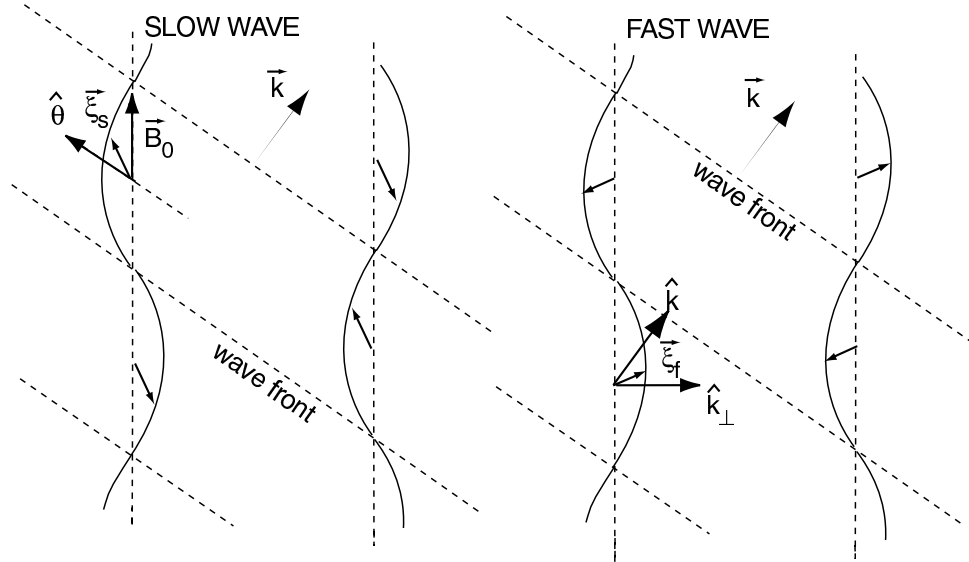


Fig. 8. Waves in real space. We show the directions of displacement vectors for a slow wave (*left*) and a fast wave (*right*). Note that $\hat{\xi}_s$ lies between $\hat{\theta}$ and \mathbf{B}_0 ($= \mathbf{k}_{\parallel}$) and $\hat{\xi}_f$ between $\hat{\mathbf{k}}$ and $\hat{\mathbf{k}}_{\perp}$. Again, $\hat{\theta}$ is perpendicular to $\hat{\mathbf{k}}$ and parallel to the wave front. Note also that, for the fast wave, for example, density (inferred by the directions of the displacement vectors) becomes higher where field lines are closer, resulting in a strong restoring force, which is why fast waves are faster than slow waves.

give schematics of slow and fast waves. For slow and fast waves, \mathbf{B}_0 , $\mathbf{v}_{\mathbf{k}}$ ($\propto \xi$), and \mathbf{k} are in the same plane. On the other hand, for Alfvén waves, the velocity of the fluid element $(\mathbf{v}_{\mathbf{k}})_A$ is orthogonal to the $\mathbf{B}_0 - \mathbf{k}$ plane.

As before, the Alfvén speed is $V_A = B_0/\sqrt{4\pi\rho_0}$, where ρ_0 is the average density. Fast and slow speeds are

$$c_{f,s} = \left[\frac{1}{2} \left\{ a^2 + V_A^2 \pm \sqrt{(a^2 + V_A^2)^2 - 4a^2 V_A^2 \cos^2 \theta} \right\} \right]^{1/2}, \quad (25)$$

where θ is the angle between \mathbf{B}_0 and \mathbf{k} . See Table 1 for the definition of other variables. When β ($\beta = P_g/P_B = 2a^2/V_A^2$; P_g = gas pressure, P_B = magnetic pressure; hereinafter $\beta = \text{average } \beta \equiv \bar{P}_g/\bar{P}_B$) goes to zero, we have

$$\begin{aligned} c_f &\approx V_A, \\ c_s &\approx a \cos \theta. \end{aligned} \quad (26)$$

Figure 7 shows directions of displacement (or, directions of velocity) vectors for these three modes. We will call them the basis vectors for these modes. The Alfvén basis is perpendicular to both $\hat{\mathbf{k}}$ and $\hat{\mathbf{B}}_0$, and coincides with the azimuthal vector $\hat{\phi}$ in a spherical-polar coordinate system. Here hatted vectors

are unit vectors. The fast basis $\hat{\xi}_f$ lies *between* $\hat{\mathbf{k}}$ and $\hat{\mathbf{k}}_\perp$:

$$\hat{\xi}_f \propto \frac{1 - \sqrt{D} + \beta/2}{1 + \sqrt{D} - \beta/2} \left[\frac{k_\perp}{k_\parallel} \right]^2 k_\parallel \hat{\mathbf{k}}_\parallel + k_\perp \hat{\mathbf{k}}_\perp, \quad (27)$$

where $D = (1 + \beta/2)^2 - 2\beta \cos^2 \theta$, and β is the averaged β ($=\bar{P}_g/\bar{P}_B$). The slow basis $\hat{\xi}_s$ lies *between* $\hat{\theta}$ and $\hat{\mathbf{B}}_0$ ($=\hat{\mathbf{k}}_\parallel$):

$$\hat{\xi}_s \propto k_\parallel \hat{\mathbf{k}}_\parallel + \frac{1 - \sqrt{D} - \beta/2}{1 + \sqrt{D} + \beta/2} \left[\frac{k_\parallel}{k_\perp} \right]^2 k_\perp \hat{\mathbf{k}}_\perp. \quad (28)$$

The two vectors $\hat{\xi}_f$ and $\hat{\xi}_s$ are mutually orthogonal. Proper normalizations are required for both bases to make them unit-length.

When β goes to zero (i.e. the magnetically dominated regime), $\hat{\xi}_f$ becomes parallel to $\hat{\mathbf{k}}_\perp$ and $\hat{\xi}_s$ becomes parallel to $\hat{\mathbf{B}}_0$ (Fig. 7b). The sine of the angle between $\hat{\mathbf{B}}_0$ and $\hat{\xi}_s$ is $(\beta/2) \sin \theta \cos \theta$. When β goes to infinity (i.e. gas pressure dominated regime)¹³, $\hat{\xi}_f$ becomes parallel to $\hat{\mathbf{k}}$ and $\hat{\xi}_s$ becomes parallel to $\hat{\theta}$ (Fig. 7c). This is the incompressible limit. In this limit, the slow mode is sometimes called the pseudo-Alfvén mode [45].

6.2 Theoretical considerations

Here we address the issue of mode coupling in a low β plasma. It is reasonable to suppose that in the limit where $\beta \gg 1$ turbulence for Mach numbers ($M_s = \delta V/a$) less than unity should be largely similar to the exactly incompressible regime. Thus, Lithwick & Goldreich [96] conjectured that the GS95 relations are applicable to slow and Alfvén modes with the fast modes decoupled. They also mentioned that this relation can carry on for low β plasmas. For $\beta \gg 1$ and $M_s > 1$, we are in the regime of hydrodynamic compressible turbulence for which no theory exists, as far as we know.

In the diffuse interstellar medium β is typically less than unity. In addition, it is ~ 0.1 or less for molecular clouds. There are a few simple arguments suggesting that MHD theory can be formulated in the regime where the Alfvén Mach number ($\equiv \delta V/V_A$) is less than unity, although this is not a universally accepted assumption. Alfvén modes describe incompressible motions. Arguments in GS95 are suggestive that the coupling of Alfvén to fast and slow modes will be weak. Consequently, we expect that in this regime the Alfvén cascade should follow the GS95 scaling. Moreover the slow waves are likely to evolve passively [96]. For $a \ll V_A$ their nonlinear evolution should be governed by Alfvén modes so that we expect the GS95 scaling for them as well. The phase velocity of Alfvén waves and slow waves depend on a factor of $\cos \theta$ and this enables modulation of the slow waves by the Alfvén ones. However, fast waves do not have this factor and therefore cannot be modulated by the changes of the magnetic field direction

¹³ In this section, we assume that external mean field is strong (i.e. $V_A > (\delta V)$) but finite, so that $\beta \rightarrow \infty$ means the gas pressure $\bar{P}_g \rightarrow \infty$.

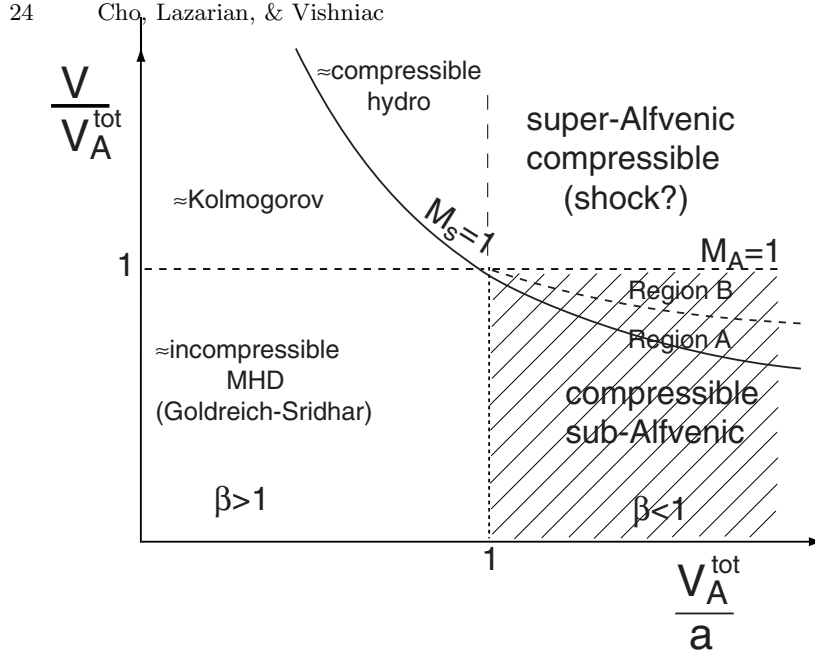


Fig. 9. Different regimes of MHD turbulence. We consider the compressible sub-Alfvénic regime (shaded region). In this figure, V_A^{tot} represents the total Alfvén speed ($= \sqrt{B_0^2 + \delta B^2} / \sqrt{4\pi\rho}$). $V \equiv V_{\text{flow}} = \delta V$. Cho & Vishniac [19] argued that, even when the external field is weak, small scales can follow the GS95-like scaling in incompressible MHD regime. Similarly, for compressible case, the small scales of super-Alfvénic compressible turbulence are expected to fall in the sub-Alfvénic compressible regime. Moreover, winding of magnetic field by turbulence increases the magnetic field energy and the super-Alfvénic turbulence becomes more and more magnetically dominated with $V/V_A \rightarrow 1$. Region B is the region where, within the density fluctuations, the velocities can get super-Alfvénic. In the figure, we used equation (33) to determine the borderline between region A and B.

associated with Alfvén waves. The coupling between the modes is through the modulation of the local Alfvén velocity and therefore is weak.

For Alfvén Mach number (M_A) larger than unity a shock-type regime is expected. However, generation of magnetic field by turbulence [19] is expected for such a regime. It will make the steady state turbulence approach $M_A \sim 1$.¹⁴ Therefore in Cho & Lazarian [21] we consider turbulence in the limit $M_s > 1$, $M_A < 1$, and $\beta < 1$ (Fig. 9). For these simulations, we mostly used $M_s \sim 2.2$, $M_A \sim 0.7$, and $\beta \sim 0.2$. The Alfvén speed of the mean external field is similar to the rms velocity ($V_A = 1, \delta V \sim 0.7, a = \sqrt{0.1}$), and we used an isothermal equation of state.

¹⁴ We suspect that simulations that show super-Alfvénic turbulence is widely spread in the ISM might not evolve for a long enough time to reach the steady state.

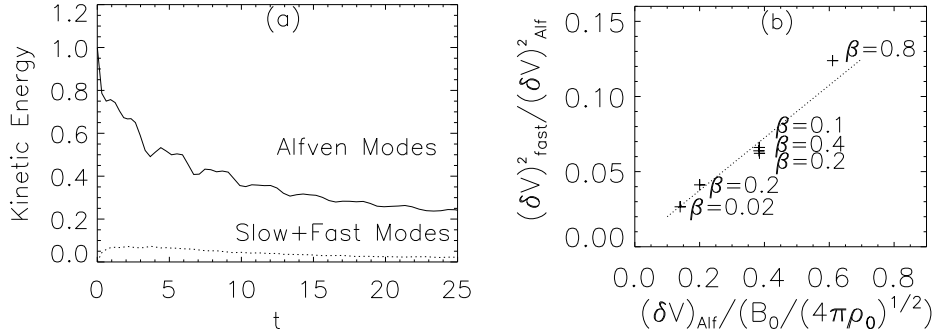


Fig. 10. (Left) Decay of Alfvénic turbulence. The generation of fast and slow waves is not efficient. $\beta \sim 0.2$, $M_s \sim 3$. (Right) The ratio of $(\delta V)_f^2$ to $(\delta V)_A^2$. The stronger the external field (B_0) is, the more suppressed the coupling is. The ratio is not sensitive to β . From [21]

Although the scaling relations presented below are applicable to sub-Alfvénic turbulence, we cautiously speculate that small scales of super-Alfvénic turbulence might follow similar scalings. Boldyrev, Nordlund, & Padoan [10] obtained energy spectra close to $E(k) \sim k^{-1.74}$ in solenoidally driven super-Alfvénic supersonic turbulence simulations. The spectra are close to the Kolmogorov spectrum ($\sim k^{-5/3}$), rather than shock-dominated spectrum ($\sim k^{-2}$). This result might imply that small scales of super-Alfvénic MHD turbulence can be described by our sub-Alfvénic model presented below, which predicts Kolmogorov-type spectra for Alfvén and slow modes.

6.3 Coupling of MHD modes and Scaling of Alfvén modes

Alfvén modes are not susceptible to collisionless damping (see [156,110] and references therein) that damps slow and fast modes. Therefore, we mainly consider the transfer of energy from Alfvén waves to compressible MHD waves (i.e. to the slow and fast modes).

In Cho & Lazarian [21], we carry out simulations to check the strength of the mode-mode coupling. We first obtain a data cube from a driven compressible numerical simulation with $B_0/\sqrt{4\pi\rho_0} = 1$. Then, after turning off the driving force, we let the turbulence decay. We go through the following procedures before we let the turbulence decay. We first remove slow and fast modes in Fourier space and retain only Alfvén modes. We also change the value of \mathbf{B}_0 preserving its original direction. We use the same constant initial density ρ_0 for all simulations. We assign a new constant initial gas pressure P_g ¹⁵. After doing all these

¹⁵ The changes of both B_0 and P_g preserve the Alfvén character of perturbations. In Fourier space, the mean magnetic field (\mathbf{B}_0) is the amplitude of $\mathbf{k} = \mathbf{0}$ component. Alfvén components in Fourier space are for $\mathbf{k} \neq \mathbf{0}$ and their directions are parallel/anti-parallel to $\hat{\xi}_A (= \hat{\mathbf{B}}_0 \times \hat{\mathbf{k}}_\perp)$. The direction of $\hat{\xi}_A$ does not depend on the magnitude of B_0 or P_g .

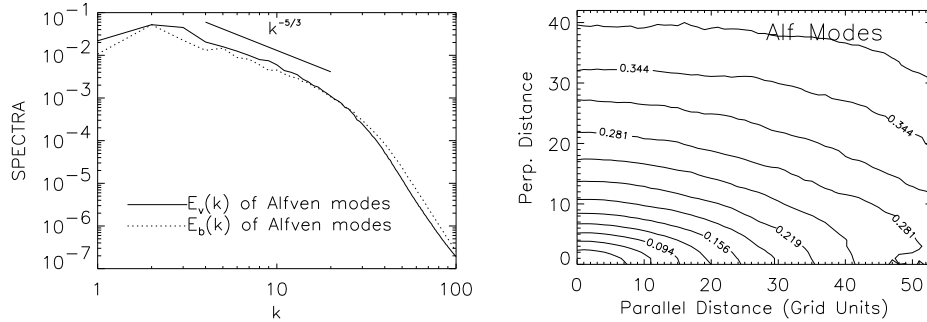


Fig. 11. (a) Alfvén spectra follow a Kolmogorov-like power law. (b) The second-order structure function ($SF_2 = \langle \mathbf{v}(\mathbf{x} + \mathbf{r}) - \mathbf{v}(\mathbf{x}) \rangle$) for Alfvén velocity shows anisotropy similar to the GS95. Contours represent eddy shapes. From [21].

procedures, we let the turbulence decay. We repeat the above procedures for different values of B_0 and P_g . Fig. 10a shows the evolution of the kinetic energy of a simulation. The solid line represents the kinetic energy of Alfvén modes. It is clear that Alfvén waves are poorly coupled to the compressible modes, and do not generate them efficiently¹⁶ Therefore, we expect that Alfvén modes will follow the same scaling relation as in the incompressible case. Fig. 10b shows that the coupling gets weaker as B_0 increases:

$$\frac{(\delta V)_f^2}{(\delta V)_A^2} \propto \frac{(\delta V)_A}{B_0}. \quad (29)$$

The ratio of $(\delta V)_s^2$ to $(\delta V)_A^2$ is proportional to $(\delta V)_A^2/B_0^2$.

This marginal coupling is in good agreement with a claim in GS95, as well as earlier numerical studies where the velocity was decomposed into a compressible component \mathbf{v}_C and a solenoidal component \mathbf{v}_S . The compressible component is curl-free and parallel to the wave vector \mathbf{k} in Fourier space. The solenoidal component is divergence-free and perpendicular to \mathbf{k} . The ratio $\chi = (\delta V)_C/(\delta V)_S$ is an important parameter that determines the strength of any shock [133,141]. Porter, Woodward, & Pouquet [138] performed a hydrodynamic simulation of decaying turbulence with an initial sonic Mach number of unity and found that χ^2 evolves toward ~ 0.11 . Matthaeus et al. [105] carried out simulations of decaying weakly compressible MHD turbulence [183] and found that $\chi^2 \sim O(M_s^2)$, where M_s is the sonic Mach number. In [10] a weak generation of compressible components in solenoidally driven super-Alfvénic supersonic turbulence simulations was obtained.

Fig. 11 shows that the spectrum and the anisotropy of Alfvén waves in this limit are compatible with the GS95 model:

$$\text{Spectrum of Alfvén Modes: } E(k) \propto k_{\perp}^{-5/3}, \quad (30)$$

¹⁶ As correctly pointed out by Zweibel (this volume) there is always residual coupling between Alfvén and compressible modes due to steepening of Alfvén modes. However, this steepening happens on time-scales much longer than the cascading time-scale.

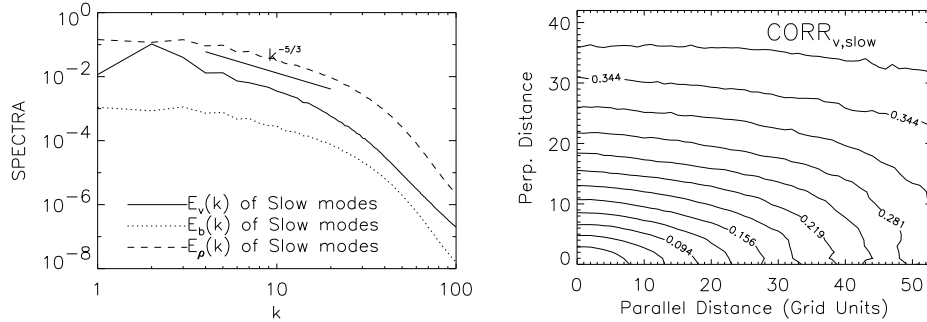


Fig. 12. (a) Slow spectra also follow a Kolmogorov-like power law. (b) Slow modes show anisotropy similar to the GS95 theory. From [21].

and scale-dependent anisotropy $k_{\parallel} \propto k_{\perp}^{2/3}$ that is compatible with the GS95 theory.

6.4 Scaling of the slow modes

Slow waves are somewhat similar to pseudo-Alfvén waves (in the incompressible limit). First, the directions of displacement (i.e. ξ_s) of both waves are similar when anisotropy is present. The vector ξ_s is always between $\hat{\theta}$ and $\hat{\mathbf{k}}_{\parallel}$. In Figure 7, we can see that the angle between $\hat{\theta}$ and $\hat{\mathbf{k}}_{\parallel}$ gets smaller when $k_{\parallel} \ll k_{\perp}$. Therefore, when there is anisotropy (i.e. $k_{\parallel} \ll k_{\perp}$), $\hat{\xi}_s$ of a low β plasma becomes similar to that of a high β plasma. Second, the angular dependence in the dispersion relation $c_s \approx a \cos \theta$ is identical to that of pseudo-Alfvén waves (the only difference is that, in slow waves, the sound speed a is present instead of the Alfvén speed V_A).

Goldreich & Sridhar [46] argued that the pseudo-Alfvén waves are slaved to the shear-Alfvén (i.e. ordinary Alfvén) waves in the presence of a strong \mathbf{B}_0 , meaning that the energy cascade of pseudo-Alfvén modes is primarily mediated by the shear-Alfvén waves. This is because pseudo-Alfvén waves do not provide efficient shearing motions. Similar arguments are applicable to slow waves in a low β plasma [21] (see also [96] for high- β plasmas). As a result, we conjecture that slow modes follow a scaling similar to the GS95 model [21]:

$$\text{Spectrum of Slow Modes: } E^s(k) \propto k_{\perp}^{-5/3}. \quad (31)$$

Fig. 12a shows the spectra of slow modes. For velocity, the slope is close to $-5/3$. Fig. 12b shows the contours of equal second-order structure function (SF_2) of slow velocity, which are compatible with $k_{\parallel} \propto k_{\perp}^{2/3}$ scaling.

In low β plasmas, density fluctuations are dominated by slow waves [21]. From the continuity equation $\dot{\rho} = \rho \nabla \cdot \mathbf{v}$

$$\omega \rho_k = \rho_0 \mathbf{k} \cdot \mathbf{v}_k, \quad (32)$$

we have, for slow modes, $(\rho_k)_s \sim \rho_0(v_k)_s/a$. Hence, this simple argument implies

$$\left(\frac{\delta\rho}{\rho}\right)_s = \frac{(\delta V)_s}{a} \sim M_s, \quad (33)$$

where we assume that $(\delta V)_s \sim (\delta V)_A$ and M_s is the Mach number. On the other hand, only a small amount of magnetic field is produced by the slow waves. Similarly, using the induction equation ($\omega\mathbf{b}_k = \mathbf{k} \times (\mathbf{B}_0 \times \mathbf{v}_k)$), we have

$$\frac{(\delta B)_s}{(\delta V)_s} \sim \frac{a}{B_0} = O(\sqrt{\beta}), \quad (34)$$

which means that equipartition between kinetic and magnetic energy is not guaranteed in low β plasmas. In fact, in Fig. 12a, the power spectrum for density fluctuations has a much larger amplitude than the magnetic field power spectrum. Since density fluctuations are caused mostly by the slow waves and magnetic fluctuation is caused mostly by Alfvén and fast modes, we *do not* expect a strong correlation between density and magnetic field, which agrees with the ISM simulations [130,126,170].

6.5 Scaling of the fast modes

Figure 13 shows fast modes are isotropic. The resonance conditions for interacting fast waves are:

$$\omega_1 + \omega_2 = \omega_3, \quad (35)$$

$$\mathbf{k}_1 + \mathbf{k}_2 = \mathbf{k}_3. \quad (36)$$

Since $\omega \propto k$ for the fast modes, the resonance conditions can be met only when all three \mathbf{k} vectors are collinear. This means that the direction of energy cascade is *radial* in Fourier space, and we expect an isotropic distribution of energy in Fourier space.

Using the constancy of energy cascade and uncertainty principle, we can derive an IK-like energy spectrum for fast waves. The constancy of cascade rate reads

$$\frac{v_l^2}{t_{cas}} = \frac{k^3 v_k^2}{t_{cas}} = \text{constant}. \quad (37)$$

On the other hand, t_{cas} can be estimated as

$$t_{cas} \sim \frac{v_k}{(\mathbf{v} \cdot \nabla \mathbf{v})_{\mathbf{k}}} \sim \frac{v_k}{\sum_{\mathbf{p}+\mathbf{q}=\mathbf{k}} k v_p v_q}. \quad (38)$$

If contributions are random, the denominator can be written by the square root of the number of interactions (\sqrt{N}) times strength of individual interactions ($\sim k v_k^2$)¹⁷. Here we assume locality of interactions: $p \sim q \sim k$. Due to the

¹⁷ To be exact, the strength of individual interactions is $\sim k v_k^2 \sin \theta$, where θ is the angle between \mathbf{k} and \mathbf{B}_0 . Thus marginal anisotropy is expected. It will be investigated elsewhere.

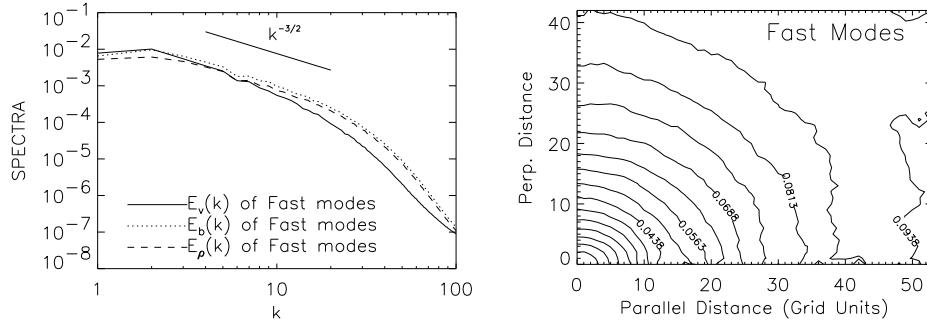


Fig. 13. (a) The power spectrum of fast waves is compatible with the IK spectrum. (b) The magnetic second-order structure function of fast modes shows isotropy. From [21].

uncertainly principle, the number of interactions becomes $\mathcal{N} \sim k(\Delta k)^2$, where Δk is the typical transversal (i.e. not radial) separation between two wave vectors \mathbf{p} and \mathbf{q} (with $\mathbf{p} + \mathbf{q} = \mathbf{k}$). Therefore, the denominator of equation (38) is $(k(\Delta k)^2)^{1/2} k v_k^2$. We obtain an independent expression for t_{cas} from the uncertainty principle ($t_{cas} \Delta \omega \sim 1$ with $\Delta \omega \sim \Delta k(\Delta k/k)$). From this and equation (38), we get $t_{cas} \sim t_{cas}^{1/2}/(k^2 v_k)$, which yields

$$t_{cas} \sim 1/k^4 v_k^2. \quad (39)$$

Combining equations (37) and (39), we obtain $v_k^2 \sim k^{-7/2}$, or $E^f(k) \sim k^2 v_k^2 \sim k^{-3/2}$. This is very similar to acoustic turbulence, turbulence caused by interacting sound waves [180,181,97]. Zakharov & Sagdeev [181] found $E(k) \propto k^{-3/2}$. However, there is debate about the exact scaling of acoustic turbulence. Here we cautiously claim that our numerical results are compatible with the Zakharov & Sagdeev scaling:

$$\text{Spectrum of Fast Modes: } E^f(k) \sim k^{-3/2}. \quad (40)$$

Magnetic field perturbations are mostly affected by fast modes [21] when β is small:

$$\text{Fast: } \frac{(\delta B)_f}{(\delta V)_A} \sim \frac{(\delta V)_f}{(\delta V)_A}, \quad (41)$$

if $(\delta V)_A \sim (\delta V)_s$.

The turbulent cascade of fast modes is expected to be slow and in the absence of collisionless damping they are expected to propagate in turbulent media over distances considerably larger than Alfvén or slow modes. This effect is difficult to observe in numerical simulations with $\Delta B \sim B_0$. A modification of the spectrum in the presence of the collisionless damping is presented in [178].

7 Astrophysical Implications

Many astrophysical problems require some knowledge of the scaling properties of turbulence. Therefore we expect a wide range of applications of the established

scaling relations. Here we show how recent breakthroughs in understanding MHD turbulence affect a few selected issues.

7.1 Cosmic ray propagation

The propagation of cosmic rays is mainly determined by their interactions with electromagnetic fluctuations in interstellar medium. The resonant interaction of cosmic ray particles with MHD turbulence has been repeatedly suggested as the main mechanism for scattering and isotropizing cosmic rays. In these analysis it is usually assumed that the turbulence is *isotropic* with a Kolmogorov spectrum (see [151]). How should these calculations be modified?

The essence of the mechanism is rather simple. Particles moving with velocity v interact with a resonant Alfvén wave of frequency $\omega = k_{\parallel}v\mu + n\Omega$ ($n = \pm 1, 2, \dots$), where $\Omega = \Omega_0/\gamma$ is the gyrofrequency of relativistic particles, μ is the cosine of the pitch angle. From the resonant condition above, we know that the most important interaction occurs at $k_{\parallel} \sim \Omega/v\mu \sim (\mu r_L)^{-1}$, where r_L is Larmor radius of the high-energy particles.

The calculations in [178] that made use of tensor (14) provided the scattering efficiency of anisotropic Alfvénic turbulence. The results are compared in Fig. 14a with the predictions of the scattering on isotropic Kolmogorov-type magnetic fluctuations and also with earlier calculations by Chandran [17]. The latter used rather *ad hoc* form of the tensor to describe magnetic fluctuations within the Goldreich-Sridhar theory. We see from Fig 14a that the scattering is substantially suppressed, compared to the Kolmogorov turbulence that is usually used for scattering calculations. This happens, first of all, because most turbulent energy in GS95 turbulence goes to k_{\perp} so that there is much less energy left in the resonance point $k_{\parallel} = (\mu r_L)^{-1}$. Furthermore, $k_{\perp} \gg k_{\parallel}$ means $k_{\perp} \gg r_L^{-1}$ so that cosmic ray particles cover many eddies during one gyration. This random walk decreases the scattering efficiency by a factor of $(\Omega/k_{\perp}v_{\perp})^{\frac{1}{2}} = (r_L/l_{\perp})^{\frac{1}{2}}$, where l_{\perp} is the turbulence scale perpendicular to magnetic field.

Thus the gyroresonance with Alfvénic turbulence is not an effective scattering mechanism for cosmic rays if turbulence is injected on the large scales, since the degree of anisotropy increases on smaller scales. However, if energy is injected isotropically at small scales, the resulting turbulence would be more isotropic and scattering will be more efficient. Scattering by undamped fast modes is more efficient than the Kolmogorov theory would predict. Yan & Lazarian [178] performed calculations taking into account the collisionless damping of fast modes and showed that the gyroresonance scattering by fast modes is the dominant scattering mechanism.

There is another important property of turbulence that was neglected in earlier work. When cosmic rays stream at a velocity much larger than Alfvén velocity, they can excite resonant MHD waves, which in turn scatter cosmic rays. This is the ‘streaming instability’. It is usually assumed that this instability can confine cosmic rays with energies less than 100GeV [16]. However, this is true only in an idealized situation when there is no background MHD turbulence. As noted earlier, the rates of turbulent decay are very fast and excited perturbations

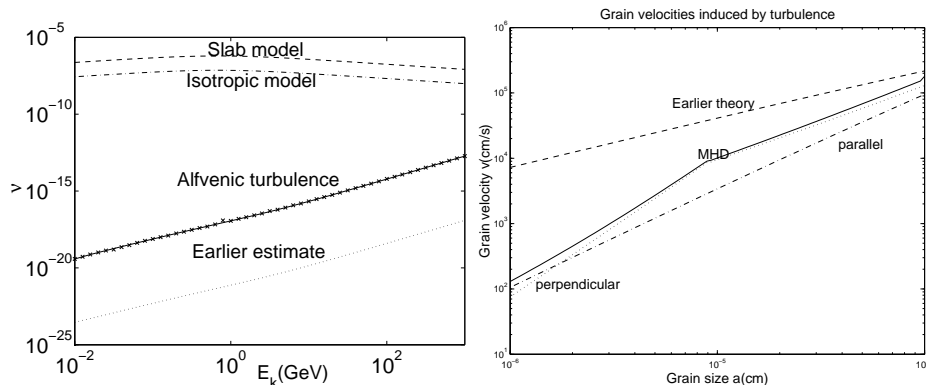


Fig. 14. Applications. (By Lazarian & Yan). *Left:* Cosmic ray scattering for realistic MHD turbulence is reduced substantially compared to scattering by isotropic turbulence, but still larger than estimates in Chandran [17]. *Right:* The dust acceleration by turbulence is reduced compared to the accepted estimates in Draine [33].

should vanish quickly. In [178] we find that the streaming instability is only applicable to particles with energies $< 0.15 GeV$, which is less than the energy of most cosmic ray particles. This result casts doubt on the self-confinement mechanism discussed by previous authors.

All these findings tend to support the alternative picture of cosmic ray diffusion advocated by Jokipii (see [69]). In this picture cosmic rays follow magnetic field lines, but the magnetic field wanders. The rate of this wandering can be calculated from the established turbulence scaling laws.

Knowledge of the scattering rates is essential for understanding both the first order and the second order Fermi acceleration. The first order Fermi acceleration, may be important for a wide range of phenomena from clusters of galaxies and gamma-ray bursts (GRBs) to solar flares. Results obtained in [178] where the discovered properties of MHD turbulence are used proved to be very different from earlier estimates.

7.2 Grain dynamics

Turbulence induces relative dust grain motions and leads to grain-grain collisions. These collisions determine grain size distribution, which affects most dust properties, including absorption and H_2 formation. Unfortunately, as in the case of cosmic rays, earlier work appealed to hydrodynamic turbulence to predict grain relative velocities (see [74,166,33,124,167,38]).

The differences between the hydrodynamic and MHD calculations stem from (a) grain charges, which couple grains to the magnetic field, (b) the anisotropy of MHD cascade, and (c) the direct interaction of charged grains with magnetic perturbations. Effects (a) and (b) are considered in Lazarian & Yan [92], while (c) is considered in Yan & Lazarian (2002b; in preparation). As consequence the picture of grain dynamics is substantially altered.

Consider grain charge first. If a grain's Larmor period $\tau_L = 2\pi m_{gr}c/qB$ is shorter than the gas drag time t_{drag} , grain perpendicular motions are constrained by magnetic field. Their velocity dispersion is determined by the turbulence eddy whose turnover period is $\sim \tau_L$ instead of the drag time [33].

Accounting for the anisotropy of MHD turbulence it is convenient to consider separately grain motions parallel and perpendicular to magnetic field. The perpendicular motion is influenced by the Alfvén modes, which have a Kolmogorov spectrum. The parallel motion is subjected to compressible modes which scale as $v_{\parallel} \propto k_{\parallel}^{-1/2}$. In addition we should account for viscous forces. When the eddy turnover time is of the order of $t_{damp} \sim \nu_n^{-1} k_{\perp}^{-2}$, the turbulence is viscously damped. Thus grains sample only a part of the eddy before gaining the velocity of the ambient gas if τ_L or $t_{drag} < t_{damp}$. The results are shown in Fig. 14b.

The direct interaction of the charged grains with turbulent magnetic field results in a stochastic acceleration that can potentially provide grains with supersonic velocities.

7.3 Turbulence in HII regions

Lithwick & Goldreich [96] addressed the issue of the origin of density fluctuations within HII regions. There the gas pressure is larger than the magnetic pressure (the 'high beta' regime) and they conjectured that fast waves, which are essentially sound waves, would be decoupled from the rest of the cascade. They found that density fluctuations are due to the slow mode and the entropy mode, which are passively mixed by shear Alfvén waves and follow a Kolmogorov spectrum. They also found that slow mode density fluctuations are proportional to $1/\sqrt{\beta}$. On the other hand, the entropy mode density fluctuations are suppressed when cooling is faster than the cascade time. Lithwick & Goldreich [96] also gave detailed discussions about density fluctuations on various scales in the ISM, e.g. proton gyro-radius. These results are important as radio-wave scintillation observations can constrain the nature of MHD turbulence in the ISM, especially in the HII regions. Lithwick & Goldreich [96] argued that the turbulent cascade survives ion-neutral damping only when a high degree of ionization is present. However, the study by Cho, Lazarian & Vishniac [24] suggests that the magnetic fluctuations protrude below the damping scale and the results of [96] should be revised.

7.4 Tiny-Scale Atomic Structures

The intermittent small scale structures in §5.2 should have important implications for transport processes (heat, cosmic rays, etc.) in partially ionized plasmas. We also speculate that they might have some relation to the tiny-scale atomic structures (TSAS). Heiles [54] introduced the term TSAS for the mysterious H I absorbing structures on scales from thousands to tens of AU, discovered by Dieter, Welch & Romney [32]. Analogs are observed in NaI and CaII [108,36,1] and in molecular gas [102]. Recently Deshpande, Dwarakanath & Goss [28] analyzed channel maps of opacity fluctuations toward Cas A and Cygnus A. They

found that the amplitudes of density fluctuations at scales less than 0.1 pc are far larger than expected from extrapolation from larger scales, possibly explaining TSAS. This study, however, cannot answer what confines those presumably overpressured (but very quiescent!) blobs of gas. Deshpande [27] related those structures to the shallow spectrum of interstellar turbulence.

Figure 5b indicates that while velocity decreases rapidly, but *not* exponentially, below the viscous damping scale, the magnetic field fluctuations persist, thereby providing nonthermal pressure support. Magnetic structures perpendicular to the mean magnetic field are compensated by pressure gradients. Our calculations so far are produced using incompressible code [24]. In the case of compressible media, we expect the pressure fluctuations to entail density fluctuations reminiscent of the Deshpande et al. [28] observations.

The calculations in Cho, Lazarian & Vishniac [24] are applicable on scales from the viscous damping scale (determined by equating the energy transfer rate with the viscous damping rate; ~ 0.1 pc in the Warm Neutral Medium with $n = 0.4 \text{ cm}^{-3}$, $T = 6000 \text{ K}$) to the ion-neutral decoupling scale (the scale at which viscous drag on ions becomes comparable to the neutral drag; $\ll 0.1$ pc). Below the viscous scale the fluctuations of magnetic field obey the damped regime shown in Figure 5b and produce density fluctuations. For typical Cold Neutral Medium gas, the scale of neutral-ion decoupling decreases to $\sim 70 \text{ AU}$, and is less for denser gas. TSAS may be created by strongly nonlinear MHD turbulence!

A simple technique of estimating magnetic field was suggested by Chandrasekhar & Fermi [18] (see also review by Ostriker, this volume). According to it, the fluctuations of magnetic field that can be measured from polarization maps are related to velocity fluctuations measured through Doppler broadening $\delta b / \sqrt{4\pi\rho} \sim \delta v$. The existence of the damped regime of MHD turbulence suggests that this technique is not applicable to very small scales in partially ionized gas.

7.5 Magnetic Reconnection

Magnetic reconnection is the fundamental process that allows magnetic fields to change their topology, despite being ‘frozen’ into highly conducting plasmas. It is the key process for solar flares, the magnetic dynamo, the acceleration of energetic particles, etc. According to the Lazarian & Vishniac model [89] (see also review [90] and Vishniac, Lazarian, & Cho, this volume) of stochastic reconnection, this process is controlled by the turbulent wandering of magnetic field. The exact properties of the turbulent cascade are especially important for the viscously damped regime present in partially ionized gas. However, it is shown in Lazarian, Vishniac & Cho [91] that the reconnection rates are sufficiently high in this case. The implications of the finding for the removal of magnetic flux during star formation is to be evaluated yet.

7.6 Support and Compression of Molecular Clouds

To understand the dynamics of molecular clouds and star formation it is necessary to understand turbulence. In a recent review [106] McKee pointed out that the fast damping of MHD turbulence observed in numerical simulations is difficult to reconcile with the fact that “a GMC such as G216, which has no visible star formation, can have a level of turbulence that exceeds that in the Rosette molecular cloud, which has an embedded OB association”. He pointed out that the conclusions obtained on the basis of numerics should be treated with caution as they do not resolve the microscales.

In typical astrophysical conditions the sources of turbulence are localized both in space (stars) and time (stellar outflows; supernovae), and the outgoing waves have much larger amplitudes than the background waves (we call this situation “imbalanced cascade”). Fig. 5a shows that the turbulent damping could be substantially reduced in this situation. Moreover, even in a balanced regime, we expect fast modes to be subjected to slow non-linear damping.

At the same time, it worth mentioning, that turbulence can not only support, but also compress molecular clouds. Clouds can be compressed by external turbulence feeding into them and depositing energy and momentum. Myers & Lazarian [120] explained observed infalling motions of molecular gas surrounding dense cores [164,94] in this way, based on ion-neutral damping. The infall rate is proportional to the rate of turbulence damping. Therefore, fast non-linear damping associated with the Alfvénic turbulence should enhance the infall.

7.7 Heating of Diffuse Ionized Gas

The “Diffuse Ionized Gas” (DIG), or equivalently the “Reynolds layer” within the Milky Way, is detected by rather faint but ubiquitous Galactic $H\alpha$ emission [144,145]. Such emission is found in several other spirals as well [142,143,127,128]. In the Galaxy, the Reynolds layer contains a substantial portion of the H^+ in the ISM. Current models generally involve photoionization from the OB stars, although how the Lyman continuum radiation from OB stars can penetrate the neutral H layer remains controversial.

The observations show strong [S II] $\lambda 6717$ and [N II] $\lambda 6583$ that increase relative to $H\alpha$ with distance z above the planes of various galaxies, including the Milky Way [145]. The only reasonable conclusion is that there is an additional source of heating in the ISM that dominates over photoionization heating at low densities. It has been proposed that carbonaceous molecules provide the excess heating through the photoelectric effect [177], but this explanation is not unique. Heating by turbulence, surely present, may dominate. Minter & Spangler [110] suggested a heating rate that is adequate to explain the [S II]/ $H\alpha$ and [N II]/ $H\alpha$ ratios, but did not take nonlinear interactions into account, thereby underestimating the heating. A new study that would capitalize on the new understanding of MHD turbulence (damping of Alfvén and fast modes, imbalance etc.) is on our agenda.

8 Observational Tests

Comparing numerics with observations is a challenging problem. Ostriker (this volume) discusses PDF, clump identification, and linewidth-scale relations as possible diagnostics and outlines problems with any of those approaches. A use of spectral line data cubes and application to it of different techniques (e.g. spectral correlation function, principal component analysis, wavelets, etc.) can be found in the review [79]. Here we shall concentrate on comparing spectra from observations with our theoretical expectations (see also review [86]).

8.1 Is the Big Power Law real?

We have mentioned above that observations suggest that the Kolmogorov power law should span from AU to kpc scales. Kolmogorov scaling is exactly what one would expect from the GS95 picture when the observations sample magnetic field in the system of reference aligned with the *mean magnetic field* (see Fig. 15 for examples of observable quantities). Indeed, it is obvious from Fig. 1 in the this system of reference (i.e. global system of reference) the locally defined scalings of k_{\parallel} with k_{\perp} are not valid. Indeed, one can easily see that the fluctuations perpendicular to the *local* direction of magnetic field dominate both the statistics measured perpendicular to the *mean* magnetic field and parallel to it. As the result in the reference system aligned with the *mean* magnetic field $k'_{\parallel} \propto k'_{\perp}$ (see Fig. 15a,b,c) and according to equation (11) $E(k) \sim k^{-5/3}$ will be measured.

Ambiguities in measurements reviewed in [2], however, make it uncertain whether or not the Big Power Law should be taken at face value. Still, we note that agreement between an observed power spectrum and theoretical expectations is far more significant than just an approximate fit between observations and numerics. The latter is definitely not unique and is *a priori* suspect in view of the huge difference in terms of Re and Rm between any numerical simulation and the ISM.

To test the Big Power Law properly, it is important to extend the theory of Velocity Channel Analysis (VCA) [84,86] by including self-absorption in the analysis of turbulent emission lines. It can then be applied to regions of HI in the inner Galaxy [30] or CO [163,162]¹⁸. Lazarian & Pogosyan [85] provided results consistent with observations. For instance, the study predicts that in the presence of absorption the emitted power in the line is proportional to k^{-3} , exactly what is seen in Dickey et al. [30] for HI in the inner region of the Galactic plane.

An application of the VCA to different emission lines (e.g. $H\alpha$, [N II], [S II] etc.) would help to answer the question of whether or not ISM turbulence is

¹⁸ Brunt & Heyer [14] applied Principal Component Analysis (see [55]), to simulated CO data and found empirical relations between the statistics of velocities, eigenvectors and eigenimages. However, they note that somehow their relation does not depend on the absorption coefficient for the limited range of absorptions they tested. Unfortunately, their analysis does not seem to be applicable to Galactic HI and the applicability of their technique to the correlated velocity and density fields is unclear.

a large scale cascade with various phases of the ISM interconnected through a dynamically important magnetic field. A contrasting possibility is that various phases form their own cascades.

HI is rather smoothly distributed across the sky. Therefore, the effects of image edges does not pose a problem for the statistical analysis. Results by Stanimirovic (private communication) show that the Fourier analysis of the SMC image and a more laborious wavelet analysis¹⁹ provide identical results. However, when dealing with molecular clouds we might expect that the cloud edges become important. Therefore the incorporation of wavelets (see [184]) within the VCA is a natural step to make. The only difference would be to apply the wavelets instead of Fourier transforms to the channel maps.

Synchrotron fluctuations and fluctuations of polarized radiation arising from aligned dust should be used to study magnetic field statistics. As we mentioned earlier Cho & Lazarian [22] has shown that those fluctuations are consistent with Kolmogorov scaling. More studies in this direction are necessary. The fact that those fluctuations interfere with the CMB studies guarantees that in the near future we shall have a lot of relevant data.

One should remember, however, that the measured power index of fluctuations may not correspond to the spectral index of the underlying turbulence. For instance, it is shown in [159] that while the actual turbulence in SMC is close to being Kolmogorov, depending on the thickness of the slice, the spectral index of intensity fluctuations within channel maps span from ~ -2.8 to ~ -3.4 . Similarly, it is shown in [22] that for Kolmogorov turbulence the spectral index of observable fluctuations may vary from ~ -1 to -3.7 depending on how observations sample turbulence.

8.2 Does turbulence reveal magnetic field direction?

Anisotropy of Alfvénic turbulence is a definite prediction of the GS95 theory. We mentioned earlier that the scale-dependent anisotropy can only be revealed in the local frame of reference, which in practical terms require direct measurements, e.g. with spacecraft. Measurements of the Solar wind magnetic turbulence have failed so far to reveal the differential scaling of the turbulence in terms of k_{\parallel} and k_{\perp} , but these measurements are inconclusive [57]. If measurement are performed in a global system of reference, as is the case with observations, they should reveal anisotropy in the direction of the mean magnetic field.

In isotropic turbulence, correlations depend only on the distance between sampling points. Contours of equal correlation are circular in this case. The presence of a magnetic field introduces anisotropy and these contours become elongated with a symmetry axis given by the magnetic field. To study turbulence anisotropy, we can measure contours of equal correlation corresponding to the data within various velocity bins. The results obtained with simulated data are shown in Fig. 15.

¹⁹ Wavelet analysis involves determining the deviation of each pixel from a weighted average of the pixels at a particular projected distance from it.

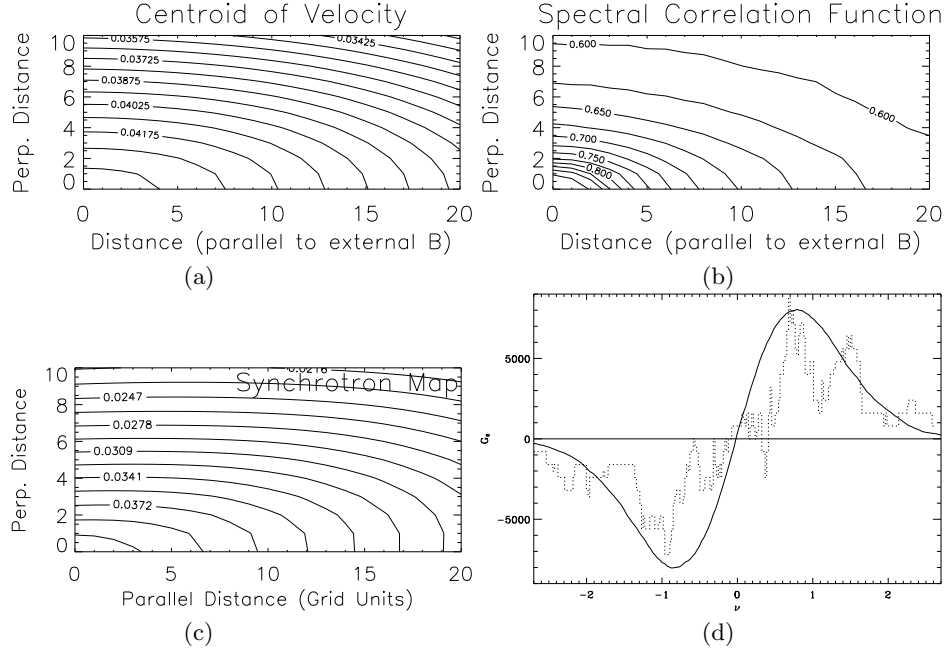


Fig. 15. *Observational test of the synthetic data by Cho, Esquivel & Lazarian.* Contours of equal correlation obtained with Centroids of Velocity ((a)) and with Spectral Correlation Function (SCF)((b)). The direction of anisotropy reveals the direction of projected magnetic field. Combined with the anisotropy analysis, the SCF (introduced by Alyssa Goodman) is likely to become even more useful tool. (c) Contours of equal correlation obtained for synthetic synchrotron intensity map. (d) shows the 2D genus of the Gaussian distribution (smooth analytical curve) against the genus for the isothermal compressible MHD simulations with Mach number ~ 2.5 (dotted curve).

Since the degree of anisotropy is related to the strength of the magnetic field, studies of anisotropy can provide the means to analyze magnetic fields. It is important to study different data sets and channel maps for the anisotropy. Optical and infrared polarimetry can benchmark the anisotropies in correlation functions. We hope that anisotropies will reveal magnetic field structure within dark clouds where grain alignment and therefore polarimetry fails (see [80] for a review of grain alignment).

Not only velocity statistics can be used for such an analysis. Lazarian & Shutenkov [83] (see review [76]) showed that the mean magnetic field must lead to anisotropies in the synchrotron statistics. Lazarian & Chibisov [81] pointed out that using HI regions as screens for radiation at the decameter wavelength it should be possible to study the 3D distribution of the magnetic field. Fig. 15c shows the anisotropy of synchrotron statistics available through simulations.

8.3 How else can we compare observations and simulations?

Velocity and density power spectra do not provide a complete description of turbulence. Intermittency (variations in the strength of the turbulent cascade) and its topology in the presence of different phases are not described by the power spectrum. Use of the higher moments is possible (see discussion of the 3 point statistics, or bispectrum, in Lazarian [79]), but is limited by the noise in the observational data.

“Genus analysis” is a good tool for studying the topology of turbulence (see the review [86]). This tool has already been successfully applied to cosmology [51]. Consider an area on the sky with contours of projected density. The 2D genus, $G(\nu)$, is the difference between the number of regions with a projected density higher than ν and those with densities lower than ν . Fig. 15d shows the 2D genus as the function of ν for a Gaussian distribution of densities (completely symmetric curve), for MHD isothermal simulations with Mach number ~ 2.5 . It is shown in [86] that the genus of the Small Magellanic Cloud is very different from that in Fig. 15d, while the spectra in both cases are similar.

9 Summary

Recently there have been significant advances in the field of MHD turbulence:

1. The first self-consistent model (GS95) of incompressible MHD turbulence that is supported by both numerical simulations and observations is now available. The major predictions of the model are scale-dependent anisotropy ($k_{\parallel} \propto k_{\perp}^{2/3}$) and a Kolmogorov energy spectrum ($E(k) \propto k^{-5/3}$).
2. There have been substantial advances in understanding compressible MHD. Simulations of compressible MHD turbulence show that there is a weak coupling between Alfvén waves and compressible MHD waves and that the Alfvén modes follow the Goldreich-Sridhar scaling. Fast modes, however, decouple and exhibit isotropy.
3. Contrary to general belief, in typical interstellar conditions, magnetic fields can have rich structures below the scale at which motions are damped by the viscosity created by neutral drag (the ambipolar diffusion damping scale).
4. These advances will have a dramatic impact on our understanding of many fundamental interstellar processes, like cosmic-ray propagation, grain dynamics, turbulent heating and molecular cloud stability.
5. New techniques, e.g. VCA, allow observational tests of the theory.

Acknowledgments: We thank Peter Goldreich, John Mathis, Steven Shore, Enrique Vazquez-Semadeni, and Huirong Yan for helpful discussions. AL and JC acknowledge the support of the NSF through grant AST-0125544. ETV acknowledges NSF grant AST-0098615. This work was partially supported by National Computational Science Alliance under AST000010N and AST010011N and utilized the NCSA SGI/CRAY Origin2000. AL thanks the LOC for their financial support. The authors thank the editors for their patience with the manuscript.

References

1. S. M. Andrews, D. M. Meyer, J. T. Lauroesch: *Astrophys. J.* **552**, L73 (2001)
2. J. W. Armstrong, B. J. Rickett, S. R. Spangler: *Astrophys. J.* **443**, 209 (1995)
3. C. Baccigalupi, C. Burigana, F. Perrotta, G. De Zotti, L. La Porta, D. Maino, M. Maris, R. Paladini: *Astron. Astrophys.* **372** 8 (2001)
4. A. Bhattacharjee, C. S. Ng, S. R. Spangler: *Astrophys. J.* **494**, 409 (1998)
5. D. Biskamp: *Nonlinear Magnetohydrodynamics* (Cambridge University Press, Cambridge, 1993)
6. D. Biskamp: *Phys. Plasmas*, **9**(4), 1486 (2002)
7. D. Biskamp, E. Schwarz: *Phys. Plasmas*, **8**(7), 3282 (2001)
8. D. Biskamp, E. Schwarz, A. Celani: *Phys. Rev. Lett.* **81** 4855 (1998)
9. S. Boldyrev: *Astrophys. J.* **569**, 841
10. S. Boldyrev, A. Nordlund, P. Padoan: astro-ph/0111345 (2002)
11. A. Brandenburg: *Astrophys. J.* **550**, 824 (2001)
12. A. Brandenburg, R. L. Jennings, A. Nordlund: *J. Fluid Mech.* **306**, 325 (1996)
13. M. Brio, C. Wu: *J. Comput. Phys.* **75**, 500, (1988)
14. C. Brunt, M. Heyer: *Astrophys. J.* in press (2002) (astro-ph/0110155)
15. F. Cattaneo, D. W. Hughes: *Phys. Rev. E.* **54**, R4532 (1996)
16. C. Cesarsky: *Annu. Rev. Astro. Astrophys.* **18**, 289 (1980)
17. B. Chandran: *Phys. Rev. Lett.* **85**(22), 4656 (2001)
18. S. Chandrasekhar, E. Fermi: *Astrophys. J.* **118**, 113 (1953)
19. J. Cho, E. T. Vishniac: *Astrophys. J.* **538**, 217 (2000a)
20. J. Cho, E. T. Vishniac: *Astrophys. J.* **539**, 273 (2000b)
21. J. Cho, A. Lazarian: *Phys. Rev. Lett.* accepted (2002) astro-ph/0205282
22. J. Cho, A. Lazarian: *Astrophys. J.* submitted (2002) astro-ph/0205284
23. J. Cho, A. Lazarian, E. T. Vishniac: *Astrophys. J.* **564**, 291 (2002a) (CLV02a)
24. J. Cho, A. Lazarian, E. T. Vishniac: *Astrophys. J.* **566**, L49 (2002b)
25. L. Del Zanna, M. Velli, P. Londrillo: *Astron. Astrophys.* **367**, 705, (2001)
26. N. F. Derby: *Astrophys. J.* **224**, 1013, (1978)
27. A. A. Deshpande: *Monthly Not. Roy. Astron. Soc.* **317**, 199 (2000)
28. A. A. Deshpande, K. S. Dwarkanath, W. M. Goss: *Astrophys. J.* **543**, 227 (2000)
29. P. H. Diamond, G. G. Craddock: *Comments on the Plasma Physics of Controlled Fusion*, **13**, 287 (1990)
30. J. M. Dickey, N. M. McClure-Griffiths, S. Stanimirovic, B. M. Gaensler, A. J. Green: *Astrophys. J.* **561**, 264 (2001)
31. R. L. Dickman: in *Protostars and Planets II*, ed. by D. C. Black, M. S. Mathews (Tucson: Univ. Arizona Press, 1985) p.150
32. N. H. Dieter, W. J. Welch, J. D. Romney: *Astrophys. J.* **206**, L113 (1976)
33. B. T. Draine: 1985, in *Protostars and Planets II*, ed. by D. C. Black, M. S. Matthews (Tucson: Univ. Arizona Press, 1985) p. 621
34. B. T. Draine, Lazarian, A.: *Astrophys. J.* **512**, 740 (1999)
35. B. G. Elmegreen: in *From Darkness to Light*, ed. by T. Montmerle, P. Andre (ASP Conf. Series, in press, 2001) (astro-ph:0010582)
36. M. D. Faison, W. M. Goss: *Astron. J.* **121**, 2706 (2001)
37. E. Falgarone, G. Pineau des Forets, E. Roueff: *Astron. Astrophys.* **300**, 870 (1995)
38. E. Falgarone, J. L. Puget, *Astron. Astrophys.* **293**, 840 (1995)
39. J. Fournier, P. Sulem, A. Pouquet: *J. Phys. A*, **15**, 1393 (1982)
40. P. Fosalba, A. Lazarian, S. Prunet, J. A. Tauber: *Astron. J.* **564**, 762 (2002)

41. U. Frisch: *Turbulence: the legacy of A.N. Kolmogorov*, (Cambridge Univ. Press, New York, 1995)
42. S. Galtier, S. V. Nazarenko, A. C. Newell, A. Pouquet: *J. Plasma Phys.* **63**, 447 (2000)
43. G. Giardino, A.J. Banday, P. Fosalba, K.M. Górski, J.L. Jonas, W. O'Mullane, J. Tauber: *Astron. Astrophys.* **371** 708 (2001)
44. G. Giardino, A.J. Banday, K.M. Górski, K. Bennett, J.L. Jonas, J. Tauber: *Astron. Astrophys. astro-ph/0202520* (2002)
45. P. Goldreich, H. Sridhar: *Astrophys. J.* **438**, 763 (1995) (GS95)
46. P. Goldreich, H. Sridhar: *Astrophys. J.* **485**, 680 (1997)
47. M. L. Goldstein: *Astrophys. J.* **219**, 700 (1978)
48. M. L. Goldstein, D. A. Roberts: *Annu. Rev. Astron. Astrophys.* **33**, 283, (1995)
49. J. Goodman, R. Narayan: *Monthly Not. Roy. Astron. Soc.* **214**, 519 (1985)
50. S. Ghosh, W. M. Matthaeus, D. C. Montgomery: *Phys. Fluids*, **31**, 2171 (1988)
51. J. R. Gott, C. Park, R. Juskiwicz, W. Bies, F. Bouchet, A. Stebbins: *Astrophys. J.* **352**, 1 (1990)
52. D. A. Green: *Monthly Not. Roy. Astron. Soc.* **262**, 328 (1993)
53. A. V. Gruzinov, P. H. Diamond: *Phys. Rev. Lett.* **72**, 1671 (1994)
54. C. Heiles: *Astrophys. J.* **481**, 193 (1997)
55. M. H. Heyer, F. P. Schloerb: *Astrophys. J.* **475**, 173 (1997)
56. J. C. Higdon: *Astrophys. J.* **285**, 109 (1984)
57. T. S. Horbury: in *Plasma Turbulence and Energetic particles*, ed. by M. Ostrowski, R. Schlickeiser (Cracow, Poland, 1999) p.28
58. T. S. Horbury, A. Balogh: *Nonlin. Proc. Geophys.* **4**, 185 (1997)
59. S. von Horner: *Zs.F. Ap.* **30**, 17 (1951)
60. M. Hossain, P. C. Gray, D. H. Pontius, W. H. Matthaeus: *Phys. Fluids*, **7**, 2886 (1995)
61. P. Iroshnikov: *Astron. Zh.* **40**, 742 (1963) (English: *Sov. Astron.* **7**, 566 (1964))
62. V. Jayanti, J. V. Hollweg: *J. Geophys. Res.* **98**, 13247 (1993)
63. K. Joulain, E. Falgarone, G. Pineau des Forets, D. Flower: *Astro. Astrophys.* **340**, 241 (1998)
64. J. Kampé de Fériet: in: *Gas Dynamics of Cosmic Clouds* (Amsterdam: North-Holland, 1955) p.134
65. S. A. Kaplan, S. B. Pickelner: *The Interstellar Medium* (Harvard Univ. Press, 1970)
66. L. Klein, R. Bruno, B. Bavassano, H. Rosenbauer: *J. Geophys. Res.* **98**, 17461 (1993)
67. R. S. Klessen: *astro-ph/0106332* (2001)
68. A. Kolmogorov: *Dokl. Akad. Nauk SSSR*, **31**, 538 (1941)
69. J. Kota, J. R. Jokipii: *Astrophys. J.* **531**, 1067 (2000)
70. R. Kraichnan: *J. Fluid Mech.* **5**, 497 (1959)
71. R. Kraichnan: *Phys. Fluids* **8**, 1385 (1965)
72. F. Krause, & K.H. Radler: *Mean-Field Magnetohydrodynamics and Dynamo Theory* (Oxford: Pergamon Press 1980)
73. R. M. Kulsrud, S. W. Anderson: *Astrophys. J.* **396**, 606 (1992)
74. T. Kusaka, T. Nakano, C. Hayashi: *Prog. Theor. Phys.* **44**, 1580 (1970)
75. R. B. Larson: *Monthly Not. Roy. Astron. Soc.* **194**, 809 (1981)
76. A. Lazarian: *Astron. and Astrophys. Transactions*, **3**, 33 (1992)
77. A. Lazarian: *Astron. Astrophys.* **293**, 507 (1995)
78. A. Lazarian: in *Interstellar Turbulence*, ed. by J. Franco, A. Carraminana (Cambridge Univ. Press, 1999a) p.95 (*astro-ph/9804024*)

79. A. Lazarian: in *Plasma Turbulence and Energetic Particles*, ed. by M. Ostrowski, R. Schlickeiser (Cracow, 1999b) p.28, (astro-ph/0001001)
80. A. Lazarian: 2000, in *Cosmic Evolution and Galaxy Formation*, ASP v.215, ed. by J. Franco, E. Terlevich, O. Lopez-Cruz, I. Aretxaga (Astron. Soc. Pacific,2000) p.69 (astro-ph/0003414)
81. A. Lazarian, G. Chibisov: *Sov. Astron. Lett.* **17**(3), 208 (1991)
82. A. Lazarian, A. Goodman, P. Myers: *Astrophys. J.* **490**, 273 (1997)
83. A. Lazarian, V. R. Shutenkov: *Sov. Astron. Lett.* **16**(4), 297 (1990)
84. A. Lazarian, D. Pogosyan: *Astrophys. J.* **537**, 720L (2000)
85. A. Lazarian, D. Pogosyan: (2002), in preparation
86. A. Lazarian, D. Pogosyan, A. Esquivel: 2002, in *Seeing Through the Dust*, ed. by R. Taylor, T. Landecker, A. Willis (ASP Conf. Series, 2002), in press (astro-ph/0112368) (LPE02)
87. A. Lazarian, D. Pogosyan, E. Vazquez-Semadeni, B. Pichardo: *Astrophys. J.* **555**, 130 (2001)
88. A. Lazarian, S. Prunet: in *Astrophysical Polarized Backgrounds*, ed. by S. Cecchini, S. Cortiglioni, R. Sault, C. Sbarra (2002) (astro-ph/0111214)
89. A. Lazarian, E. T. Vishniac: *Astrophys. J.* **517**, 700 (1999)
90. A. Lazarian, E. T. Vishniac: in *Astrophysical Plasmas: Codes, Models, and Observations*, eds. by J. Arthur, N. Brickhouse, & J. Franco, *RevMexAA (Serie de Conferencias)*, Vol. **9**, 55
91. A. Lazarian, E. T. Vishniac, J. Cho: 2002, in preparation
92. A. Lazarian, H. Yan: *Astrophys. J.* **566**, 105 (2002)
93. R. J. Leamon, C. W. Smith, N. F. Ness, W. H. Matthaeus: *J. Geophys. Res.* **103**, 4775 (1998)
94. C. W. Lee, P. C. Myers, M. Tafalla: *Astrophys. J. Supp.* **136**, 703 (2001)
95. M. Lesieur: *Turbulence In Fluids* (Dordrecht: Kluwer, 1990)
96. Y. Lithwick, P. Goldreich: *Astrophys. J.* **562**, 279 (2001)
97. V. S. L'vov, Y. V. L'vov, A. Pomyalov: *Phys. Rev. E*, **61**, 2586 (2000)
98. M. Mac Low: *Phys. Rev. Lett.* **80**, 2754 (1998)
99. M. Mac Low: *Astrophys. J.* **524**, 169 (1999)
100. J. Maron, S. Cowley: astro-ph/0111008 (2001)
101. J. Maron, P. Goldreich: *Astrophys. J.* **554**, 1175 (2001)
102. A. P. Marscher, E. M. Moore, T. M. Bania: *Astrophys. J.* **419**, L101 (1993)
103. W. M. Matthaeus, M. L. Goldstein, D. C. Montgomery: *Phys. Rev. Lett.* **51**, 1484 (1983)
104. W. M. Matthaeus, S. Oughton, S. Ghosh, M. Hossain: *Phy. Rev. Lett.* **81**, 2056 (1998)
105. W. M. Matthaeus, S. Ghosh, S. Oughton, D. A. Roberts: *J. Geophys. Res.* **101**, 7619 (1996)
106. C. F. McKee: in *The Origin of Stars and Planetary Systems*, ed. by J. L. Charles, D. K. Nikolaos (Dordrecht: Kluwer, 1999) p.29
107. M. Meneguzzi, U. Frish, A. Pouquet: *Phys. Rev. Lett.* **47**, 1060 (1981)
108. D. M. Meyer, J. C. Blades: *Astrophys. J.* **464**, L179 (1996)
109. L. J. Milano, W. H. Matthaeus, P. Dmitruk, D. C. Montgomery: *Phys. Plasmas*, **8**(6), 2673 (2001)
110. A. Minter, S. Spangler: *Astrophys. J.* **485**, 182 (1997)
111. H. K. Moffatt: *Magnetic Field Generation in Electrically Conducting Fluids* (Cambridge: Cambridge Univ. Press, 1978)
112. A. S. Monin, A. A. Yaglom: *Statistical Fluid Mechanics: Mechanics of Turbulence*, Vol. 2 (Cambridge: MIT Press, 1975)

113. D. C. Montgomery: *Physica Scripta*, **T2/1**, 83 (1982)
114. D. C. Montgomery, W. H. Matthaeus: *Astrophys. J.* **447**, 706 (1995)
115. D. C. Montgomery, L. Turner: *Phys. Fluids* **24**(5), 825 (1981)
116. W.-C. Müller, D. Biskamp: *Phys. Rev. Lett.* **84**(3) 475 (2000)
117. G. Munch: *Rev. Mod. Phys.* **30**, 1035 (1958)
118. P. C. Myers: *Astrophys. J.* **270**, 105 (1983)
119. P. C. Myers: in *The Origin of Stars and Planetary Systems*, ed. by J. L. Charles, D. K. Nikolaos (Dordrecht: Kluwer, 1999) p.67
120. P. C. Myers, A. Lazarian: *Astrophys. J. Lett.* **507**, 157 (1998)
121. R. Narayan, J. Goodman: *Monthly Not. Roy. Astron. Soc.* **238**, 963 (1989)
122. C. S. Ng, A. Bhattacharjee: *Astrophys. J.* **465**, 845 (1996)
123. A. Nordlund, A. Brandenburg, R. Jennings, M. Rieutord, J. Ruokolainen, R. Stein, I. Tuominen: *Astrophys. J.* **392**, 647 (1992)
124. V. Ossenkopf: *Astron. Astrophys.* **280**, 617 (1993)
125. E. C. Ostriker, C. F. Gammie, J. M. Stone: *Astrophys. J.* **513**, 259 (1999)
126. E. C. Ostriker, J. M. Stone, C. F. Gammie: *Astrophys. J.* **546**, 980 (2001)
127. B. Otte, R.-J. Dettmar: *Astron. Astrophys.* **343**, 705 (1999)
128. B. Otte, R. J. Reynolds, J. S. Gallagher III, A. M. N. Ferguson: *Astrophys. J.* **560**, 207O (2001)
129. S. Oughton, E. R. Priest, W. H. Matthaeus: *J. Fluid Mech.* **280**, 95 (1994)
130. P. Padoan, A. Nordlund: *Astrophys. J.* **526**, 279 (1999)
131. P. Padoan, A. Goodman, B. T. Draine, M. Juvela, A. Nordlund, O. Rognvaldsson: *Astrophys. J.* **559**, 1005 (2001)
132. E. N. Parker: *Cosmical magnetic fields: Their origin and their activity* (Oxford University Press, New York, 1979)
133. T. Passot, A. Pouquet, P. Woodward: *Astron. Astrophys.* **197**, 228 (1988)
134. T. Passot, E. Vazquez-Semadeni, A. Pouquet: *Astrophys. J.* **455**, 536 (1995)
135. H. Politano, A. Pouquet: *Phys. Rev. E* **52**(1), 636 (1995)
136. H. Politano, A. Pouquet, V. Carbone: *Europhys. Lett.* **43**(5), 516 (1995)
137. H. Politano, A. Pouquet, P. L. Sulem: *Phys. Plasmas* **2**(8), 2931 (1995)
138. D. Porter, P. Woodward, A. Pouquet: *Phys. Fluids* **10**, 237 (1998)
139. A. Pouquet, U. Frish, J. Léorat: *J. Fluid Mech.* **77**, 321 (1976)
140. A. Pouquet, G. S. Patterson: *J. Fluid Mech.* **85**, 305 (1978)
141. A. Pouquet: in *Interstellar Turbulence*, ed. by J. Franco, A. Carraminana (Cambridge Univ. Press, 1999) p.87
142. R. J. Rand, S. R. Kulkarni, J. J. Hester: *Astrophys. J.* **352**, 1 (1990)
143. R. J. Rand: *Pub. Astro. Soc. Aust.* **15**, 106 (1998)
144. R. J. Reynolds: *Astrophys. J.* **333**, 341 (1988)
145. R. J. Reynolds, L. M. Haffner, S. L. Tufte: *Astrophys. J.* **525**, 21 (1999)
146. M. N. Rosenbluth, D. A. Monticello, H. R. Strauss, R. B. White: *Phys. Fluids* **19**, 1987 (1976)
147. D. Ryu, T. W. Jones: *Astrophys. J.* **442**, 228 (1995)
148. J. Saur, H. Politano, A. Pouquet, W. H. Matthaeus: American Geophysical Union, Fall Meeting (2001)
149. J. M. Scalo: *Astrophys. J.* **277**, 556 (1984)
150. J. M. Scalo: in *Interstellar Processes*, ed. by D. J. Hollenbach, H. A. Thronson (Dordrecht: Reidel, 1987) p.349
151. A. Schlickeiser, J. A. Miller: *Astrophys. J.* **492**, 352 (1998)
152. Z.-S. She, E. Leveque: *Phys. Rev. Lett.* **72**(3), 336 (1994) (S-L)
153. J. V. Shebalin, W. H. Matthaeus, D. C. Montgomery: *J. Plasma Phys.* **29**, 525 (1983)

154. J. H. Simonetti, J. M. Cordes: in *Radio wave scattering in the interstellar medium; Proceedings of the AIP Conference* (American Institute of Physics, New York, 1988) p. 134
155. J. H. Simonetti: *Astrophys. J.* **386**, 170 (1992)
156. S. R. Spangler: *Astrophys. J.* **376**, 540 (1991)
157. S. R. Spangler, C. R. Gwinn: *Astrophys. J.* **353**, L29 (1990)
158. S. Sridhar, P. Goldreich: *Astrophys. J.* **432**, 612 (1994)
159. S. Stanimirovic, A. Lazarian: *Astrophys. J.* **551**, L53 (2001)
160. J. M. Stone, E. C. Ostriker, C. F. Gammie: *Astrophys. J.* **508**, L99 (1998)
161. H. R. Strauss: *Phys. Fluids*, **19**, 134 (1976)
162. J. Stutzki: in *Plasma Turbulence and Energetic particles*, ed. by M. Ostrowski, R. Schlickeiser (Cracow, 1999) p.48
163. J. Stutzki, F. Bensch, A. Heithausen, V. Ossenkopf, M. Zielinsky: *Astron. Astrophys.* **336**, 697 (1998)
164. M. Tafalla, D. Mardones, P. C. Myers, P. Caselli, R. Bachiller, B. J. Benson: *Astrophys. J.* **504**, 900 (1998)
165. A. Ting, W. M. Matthaeus, D. C. Montgomery: *Phys. Fluids*, **29**, 3261 (1986)
166. H. J. Volk, F. C. Jones, G. E. Morfill, S. Roser: *Astron. Astrophys.* **85**, 316 (1980)
167. S. J. Weidenschilling, T. V. Ruzmaikina: *Astrophys. J.* **430**, 713 (1994)
168. E. Vazquez-Semadeni, T. Passot, A. Pouquet: *Astrophys. J.* **441**, 702 (1995)
169. E. Vazquez-Semadeni, T. Passot, A. Pouquet: *Astrophys. J.* **473**, 881 (1996)
170. E. Vazquez-Semadeni: in *Seeing Through the Dust*, ed. by R. Taylor, T. Landecker, A. Willis (ASP: San Francisco, 2002) (astro-ph/0201072)
171. A. Warhaft: *Annu. Rev. Fluid Mech.* **32**, 203 (2000)
172. O. C. Wilson, G. Munch, E. M. Flather, M. F. Coffeen: *Astrophys. J. Supp.* **4**, 199 (1959)
173. S. I. Vainstein, F. Cattaneo: *Astrophys. J.* **393**, 165 (1992)
174. M. K. Verma: *Phys. Plasmas*, **6**(5), 1455, (1999)
175. M. K. Verma, G. Dar, V. Eswaran: *Phys. Plasmas*, **9**(4), 1484 (2002)
176. E. T. Vishniac, J. Cho: *Astrophys. J.* **550**, 752 (2001)
177. J. C. Weingartner, B. T. Draine: *Astrophys. J. Supp.* **134**, 263 (2001)
178. H. Yan, A. Lazarian: *Phys. Rev. Lett.* submitted (2002) astro-ph/0205285
179. H. Yan, A. Lazarian: in preparation (2002)
180. V. E. Zakharov: *Sov. Phys. JETP*, **24**, 455 (1967)
181. V. E. Zakharov, A. Sagdeev: *Sov. Phys. Dokl. textbf15*, 439 (1970)
182. G. P. Zank, W. H. Matthaeus: *J. Plasma Phys.* **48**, 85 (1992)
183. G. P. Zank, W. H. Matthaeus: *Phys. Fluids A* **5**(1), 257 (1993)
184. M. Zielinsky, J. Stutzki: *Astron. Astrophys.* **347**, 630 (1999)
185. E. G. Zweibel, C. Heiles: *Nature*, **385**, 131 (1997)